Journal of Sound and Vibration (2002) **258**(2), 203–232
doi:10.1006/jsvi.2001.4214, available online at http://www.idealibrary.com on IDEAL®

ACTIVE CONTROL OF ENVIRONMENTAL NOISE, VII: PERFORMANCE OF MULTI-FREQUENCY, MULTI-CHANNEL, FREEFIELD SOUND CANCELLING SYSTEMS

S. E. Wright and H. Atmoko

School of Engineering, University of Huddersfield, Huddersfield HDI 3DH, England.
E-mail: selwyn.wright@ntworld.com

(*Received* 11 *June* 2001, *and in final form* 28 *November* 2001)

The paper considers the performance of multi-frequency, multi-channel, freefield sound cancelling systems for the reduction of discrete frequency and periodic noise. The approach uses a method of directional active noise control. Large sound reductions from these systems have been made possible through: (a) synthetically generating the cancelling sound and synchronizing with the primary source; (b) automatic alignment of all stability regions of the control system; and (c) avoiding instability produced by these multi-channel systems.

1. INTRODUCTION

1.1. THE NEED

Historically, it has been difficult to obtain significant active noise reduction from a primary source over appreciable large regions (greater than a fraction of an acoustic wavelength). However, large cancellations have been obtained over considerable distances using a divergent arrangement of basic cancelling units in an electronically controlled acoustic shadow (ECAS) configuration [1]. The paper focuses on the reduction of predictable discrete frequency noise and multiples of discrete frequencies (periodic noise), which is one of the main causes of industrial annoyance and hearing loss. The physical and acoustical principles involved in generating these large cancellation regions and many of the processing techniques developed in this work are equally relevant to the cancellation of other more complex forms of noise, including unpredictable noise. However, the speed and quality of the adaptive algorithm and the processing power, limit the present applications to predictable noise.

In many walks of life there is excessive noise. There is an enormous potential for economic and social benefit in succeeding in this development. It will help to reduce environmental noise pollution continually increasing from industry, construction, transportation and domestic noise sources. It will help meet ever increasingly stringent noise regulations. There is the potential to reduce sound, which is very hard using conventional methods, where at present very heavy and expensive structures are required. This opens up the whole field of reducing noise from machinery, such as large generators/motors, diesel engines, construction sites, earth moving vehicles, factory machinery and mills (most of which now have to operate 24 h per day to remain competitive—which in turn causes noise problems at night).

0022-460X/02/$35.00

1.2. THE APPROACH

The project is to do with sound reduction using a directional active-noise control (ANC) technique. Active-noise control is concerned with reducing sound by combining it with a negative replica (sound of the opposite phase and same amplitude). The project involves generating an acoustic shadow (quiet zone), from noisy equipment, in the direction of a sensitive or complaint area. This method is capable theoretically of producing large quiet regions extending to infinity; in practice, at least to large distances [1]. The cancelling system has intelligence in that it can absorb selectively the unwanted sound and leave other wanted sounds unchanged. It has the potential to outperform conventional classical sound blocking systems, with the ability to generate the perfect shadow, without acoustic leakage (diffraction). The system has no difficulty producing shadows across complex sound fields radiated by large primary sources [2].

The shadow is constructed from a number of basic cancelling units (phase controlled dipoles) [3, 4]. Here a basic acoustic shadow is generated in the direction of the successive alignment of the primary source, secondary source (cancelling loud speaker) and detection system (error microphone), with the appropriate amplitude and phasing of the secondary source to produce a minimum at the microphone. The resulting sound directivity can be a four-leaf clover, figure-of-eight or heart-shaped, depending on the source separation distance of a whole, half or quarter wavelength respectively. For maximum cancellation, the primary and secondary sources should be as close together as possible and the detection system as far away as practical, there are no optimum distances. The shadow, once formed at the detector, can then propagate to large distances.

To produce effective shadows over a substantial angle from a non-compact primary source (wavelength smaller than the source size), a diverging array of these basic cancelling systems are arranged within shadow control angles. From the information it receives from the detectors, after digital signal processing, the secondary speaker outputs are adjusted appropriately, both in phase and amplitude, to minimize the sound at the detectors [5]. The combined effect is to produce a deep sharp shadow, confined within the control angles. The system has the ability to adapt automatically to maintain its shadow depth and direction, through environmental changes [6]. The structure can be unobtrusive, noise selective, light, easily removed and flexible in design, simply reconfigured to a new application, or upgraded to meet more stringent noise legislation. The theory predicts considerable attenuation, and measurement now supports the conclusion that effective robust systems can be built. Shadows >40 dB (one hundreth of the original sound) have been measured experimentally for discrete frequencies, confirming the viability. This is a very significant achievement compared to attenuation achieved previously.

1.3. A BRIEF HISTORY

Lueg in 1936 [7] was the first person to patent the concept of active noise control in reducing sound in ducts. His idea was to measure noise at one point in the duct and inject it at an antiphase point (half wavelength down the duct). However, he did not have the sophisticated hardware to implement his ideas. It was not until 1953, 17 years later, before Olson and May [8] attempted to cancel sound in open space using amplified controlled sound. Chaplin and Smith in 1979 [9] patented the first sophisticated algorithms to control sound in a duct. In 1985, Widrow and Searns [10] published details of the famous filtered x algorithm and Elliott *et al.* [11] in 1987 developed the now famous multi-channel algorithm to cancel sound in enclosures. Wright and Angevine [12] in 1990 published the

concept of electronically controlled acoustic shadows. Kuo and Morgan [13] assembled all the recorded major active noise control work in one book in 1996. Finally, very recently Elliott [14] in 2001, has considered the signal processing principles involved in active noise control. Currently, most of the research work in active noise control is being carried out in enclosures, such as ducts, jet engines, fighter pilots headsets, car, truck and aircraft cabins, where moderate success has been obtained.

1.4. UNBOUNDED SPACE

The success of the present work in unbounded space has been made possible through the following developments described in detail in references [1–6]:

(a) Recognition that freefield systems could be superior to systems in enclosures, where complex diffuse/resonant fields limit their quiet zone to within a fraction of an acoustic wavelength. Whereas, in freefield systems, with the appropriate geometry, the quiet zone can extend to infinity, theoretically, no matter what the frequency.
(b) Establishment of freefield directional ANC systems which can form acoustic shadows within control angles and adjust automatically in a co-ordinated manner. These systems have intelligence and the potential to outperform conventional sound blocking systems, producing optimum shadows without classical diffraction.
(c) Detailed understanding of the generation, interference and cancellation of complex acoustic fields from discrete source arrays, including the characterization of near and far field, which is fundamental to discrete source cancellation systems.
(d) Realization of the stability process of freefield systems, in terms of orbital poles circulating around cancelling zeros defining a set of stability bands, thus allowing the optimum adaptive performance, in terms of cancellation depth, adaptive speed and spectral purity to be understood and implemented.
(e) Establishment of robustness criteria of multi-channel freefield systems in terms of sum and difference eigenspectra and identifying multiple instability peaks that have to be avoided, if these systems are to convert effectively.
(f) Method of automatically identifying, centring and aligning the stability bands of a multi-frequency, multi-channel freefield system.
(g) Establishing the effect of three-dimensional sources, reflections and cross wind on the freefield shadow and the effect of environmental change on the control system stability.

Rather than attempting to investigate complex sources and cancellation systems in the time domain, it was recognized that it would be more expedient to establish the discrete frequency performance of the basic "canceller" in the frequency domain and then investigate multi-frequency and multi-channel systems.

1.5. FUTURE SUCCESS

Success in cancelling steady periodic noise is high, and less probable with unsteady predictable noise. The number of uncertainties increases with source variations, environmental changes and topological changes. However, initial computer modelling of the techniques used here predicts sufficient attenuation to overcome deterioration through most practical variations. Providing these variations are not severe, it is anticipated that the adaptive process will follow them. In severe weather conditions outdoors, the ANC system should not be needed and could shut down automatically. In large factory spaces most of these variations are absent.

Reducing unpredictable noise, such as broadband random noise, speech and music, is a higher risk. Although the shadow mechanism is governed by the same propagation and cancellation physics as predictable noise, the accurate synthesis or copying of the primary

source for generating the cancelling sound, in real time, is more demanding. The success depends critically on the algorithm adaptive accuracy, speed and computational efficiency.

1.6. THE CONTENTS

The properties of the basic freefield cancelling system are considered in detail in reference [4]. Details of multi-frequency cancelling systems, based on one of these basic "cancellers", are now discussed in section 2.

The control conditions necessary for multi-channel systems to operate effectively are considered in section 3. The adaptive convergence characteristics and the overall adaptive speed of these multi-channel systems are then established in section 4.

Finally, the acoustic directivities, shadow profile and shadow depth are considered in section 5. Here, the shadows are compared with theoretical predictions using wave theory computer-generated acoustic fields.

2. PERIODIC NOISE

To cancel multi-frequency (periodic) noise from a primary source, one can use a microphone directly to measure the primary sound, and then after processing, use the signal to cancel the primary noise. The problem with this approach is that the system is potentially unstable through feedback generated by the secondary sound being picked up by the measuring microphone. Also, the multi-tap FIR filters used to cancel the sound are slow to adapt to primary source changes, making this approach unsuitable for rapidly changing periodic noise. An alternative, more robust method, is to remove the feedback loop altogether and use multi-2-tap FIR filters. This not only removes the potential instability, it drastically improves the adaptive speed and considerably improves the signal-to-noise ratio to give better cancellation.

2.1. PHASE-LOCK LOOP

The approach is to synthesize the sound and synchronize it to the primary source indirectly, using a phase-lock loop technique [15, 16]. Figure 1 illustrates the system. At the top left-hand side of the figure is shown an acoustic, vibration or an electromagnetic sensor that monitors a representation of the primary source signal. This signal is first passed through a frequency-seeking procedure, where the source signal is discretely Fourier transformed (DFT). The fundamental frequency is then selected, usually the largest harmonic (or any harmonic can be selected). This frequency is then used to set the initial frequency of the synthetic signal generator (digital voltage controlled oscillator VCO) implemented in software. An adaptive loop (amplitude regulator) is placed in series with the primary source measuring transducer to limit the signal levels to those within the operating range of the VCO.

The output from the oscillator is then multiplied (cross-correlated) with the output from the source sensor to form a second adaptive loop. The product, which contains sum and difference frequencies of the two signals, is fed through a low-pass filter. The resulting low-frequency component (time-varying DC voltage, V,) is then used to change the frequency of the VCO. The output from the VCO is continuously updated until its frequency becomes identical to the primary source signal, in which case the DC output, V, from the LP filter, reduces to zero. In this way, the synthetic oscillator can keep track automatically of source frequency changes.

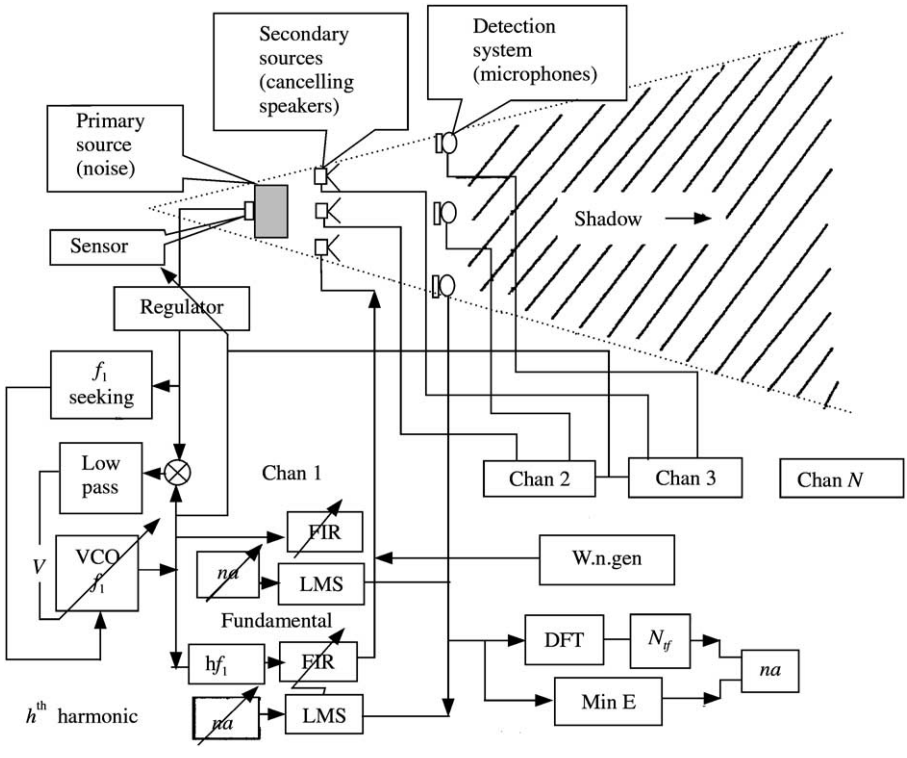

Figure 1. Electronically controlled acoustic shadow system.

If the signals from the primary source sensor and the synthetic oscillator are respectively

$$P(t) = A_p \cos(\omega_p t + \phi_p), \quad O(t) = A_0 \sin(\omega_0 t + \phi_0), \tag{1}$$

then the output from the multiplier becomes

$$V_x = MP(t)O(t) = K_x\{\sin[(\omega_0 - \omega_p)t + \phi_0 - \phi_p] + \sin[(\omega_0 + \omega_p)t + \phi_0 + \phi_p]\}. \tag{2}$$

where M is the multiplier constant and ω_p,ϕ_p and ω_0,ϕ_0 are the angular frequencies and phases of the synthetic oscillator and primary source respectively. After low-pass filtering, equation (2) becomes

$$V_x = K_x \sin\theta, \tag{3}$$

where

$$K_x = M\ A_p A_0/2 \quad \text{and} \quad \theta = (\omega_0 - \omega_p)t + \phi_0 - \phi_p\,.$$

The VCO angular frequency output is then given by

$$\omega_0 = \omega_i + \mathrm{d}\omega, \qquad \mathrm{d}\omega = K_0 V_f = K_0 K_x \sin\theta. \tag{4}$$

Here ω_0 and ω_i are the updated and previous angular frequency values of the oscillator, respectively, $\mathrm{d}\omega$ is the updating frequency and K_0 is the VCO conversion constant. When $\theta = 0$, $V_x = 0$, $\mathrm{d}\omega = 0$ and $\omega_0 = \omega_i = \omega_p$.

The hold frequency range $\mathrm{d}\omega_h$, where the VCO can be "pulled" from the primary source frequency and stay adaptive is determined by $|\sin\theta| = 1$. Also the capture range $\mathrm{d}\omega_c$, where the VCO frequency is sufficiently close to the primary source frequency to adapt, together

with $d\omega_h$, are given, respectively, by

$$d\omega_h = \pm K_0 K_x, \quad d\omega_c = \pm \omega_{lpbw}, \tag{5}$$

where ω_{lpbw} is the low-pass bandwidth of the filter.

2.2. CANCELLING SYSTEM

The output from the VCO finally drives the secondary cancelling loudspeaker through a third adaptive loop containing the FIR 2-tap LMS adaptive filter. This filter adjusts automatically to minimize the signal at the error microphone. Also, shown in Figure 1 is a series of single harmonic generators used in parallel to cancel multi-frequency (periodic) noise, the harmonics being a series of multiples, h, of the fundamental frequency f_1.

Each harmonic requires the correct loudspeaker–microphone propagation distance delay compensation sample number n_a, to assure mid-stability band operation. This is achieved through the blocks illustrated in the bottom right-hand corner of Figure1. Initially, white noise is injected at each speaker successively and the impulse response measured between each speaker–microphone combination to measure each individual control loop transfer function. The DFT process is applied to obtain the phase transfer function N_{tf}, in terms of multiples of 2π, of the ANC system. The n_a number is then calculated from the N_{tf} to set each adaptive loop in the centre of its stability band.

After the initial stability band positioning, each loop is kept operating in its mid-band position, through environmental changes, by implementing a fourth adaptive loop. Here, the n_a number is adjusted automatically, through a combination of the following: (1) minimizing the error signal at the detection microphones; (2) minimizing the drive signal to the speakers; or (3) minimizing the filter tap (coefficient) change, all of which indicate mid-stability band operation. This whole operating system is programmed in C.

2.3. MEASURED DATA

Figure 2 shows the time histories and frequency-domain signatures for a single channel. The primary source is driven by a periodic signal generated by a triangular waveform. Figure 2(a) gives the signals at the monitoring microphone before cancellation (fundamental frequency plus two harmonics). Figure 2(b) shows the active noise signals at the cancelling loudspeaker. Figure 2(c) shows the cancelled (residual error) signals at the microphone. In the time domain, the cancelled sound is at least 10 times smaller than the uncancelled sound (20 dB reduction), the remaining sound being uncorrelated LF wind noise. In the frequency domain all three primary source frequencies have been cancelled almost completely simultaneously.

3. MULTI-CHANNEL SYSTEMS

To reduce sound from large sources over substantial angles requires large channel number systems. The multi-frequency systems discussed in section 2 are duplicated to control sound from an array of secondary cancelling loud speakers and detection microphones contained within the shadow control angles, as illustrated in Figure 1.

3.1. MULTI-CHANNEL STRUCTURE

Figure 3 shows the details of a multi-channel system (four channels in this case). The phase-lock loop (PLL) drives each harmonic frequency "canceller", which, as described

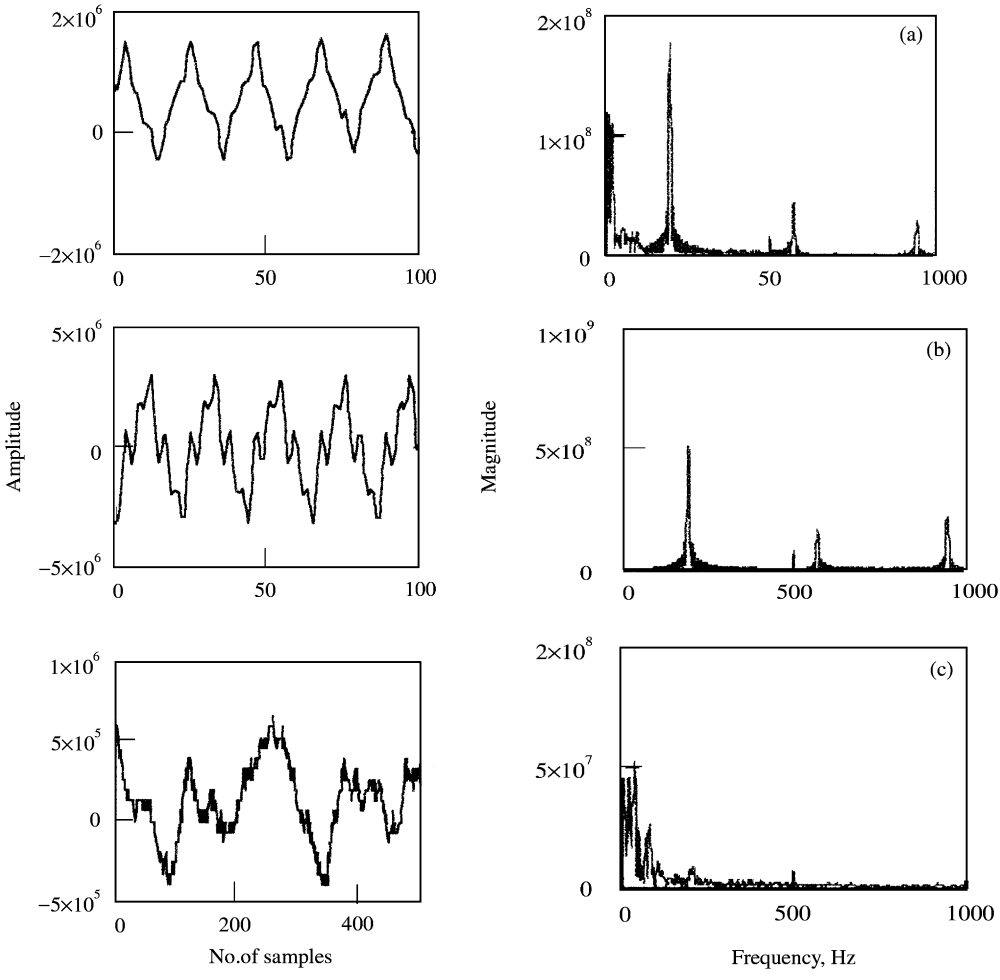

Figure 2. Cancellation of multi-frequencies (periodic noise): (a) uncancelled sound; (b) cancelling sound; and (c) cancelled sound (error).

earlier in section 2 are multiples h of the fundamental frequency (f_1). For each harmonic, the signal (Y) drives the loud speaker through an adaptive filter (W). Each filter W is a 2-tap (coefficient) filter whose taps are driven by references X_0 and X_1 (90° out of phase with X_0) through D_{90}. Each delayed LMS algorithm requires outputs (E) from all error microphones (m). They are also driven from the references $\mathbf{X}_0$ and X_1 through the propagation delay elements (C_{sm}) representing the propagation space between each speaker and microphone.

The relationships between these quantities are for the first channel:

$$Y_1 = W_{10}X_0 + W_{11}X_1,\ X_0 \text{ is } 90^\circ \text{ out of phase with } X_1,$$

$$W_{10} = W_{10} - \mu E_1 C_{11}\mathrm{X}_0 - \mu E_2 C_{12} X_0 - \mu E_3 C_{13} X_0 - \mu E_4 C_{14} X_0,$$

$$W_{11} = W_{11} - \mu E_1 C_{11} X_1 - \mu E_2 C_{12} X_1 - \mu E_3 C_{13} X_1 - \mu E_4 C_{14} X_1, \qquad (6)$$

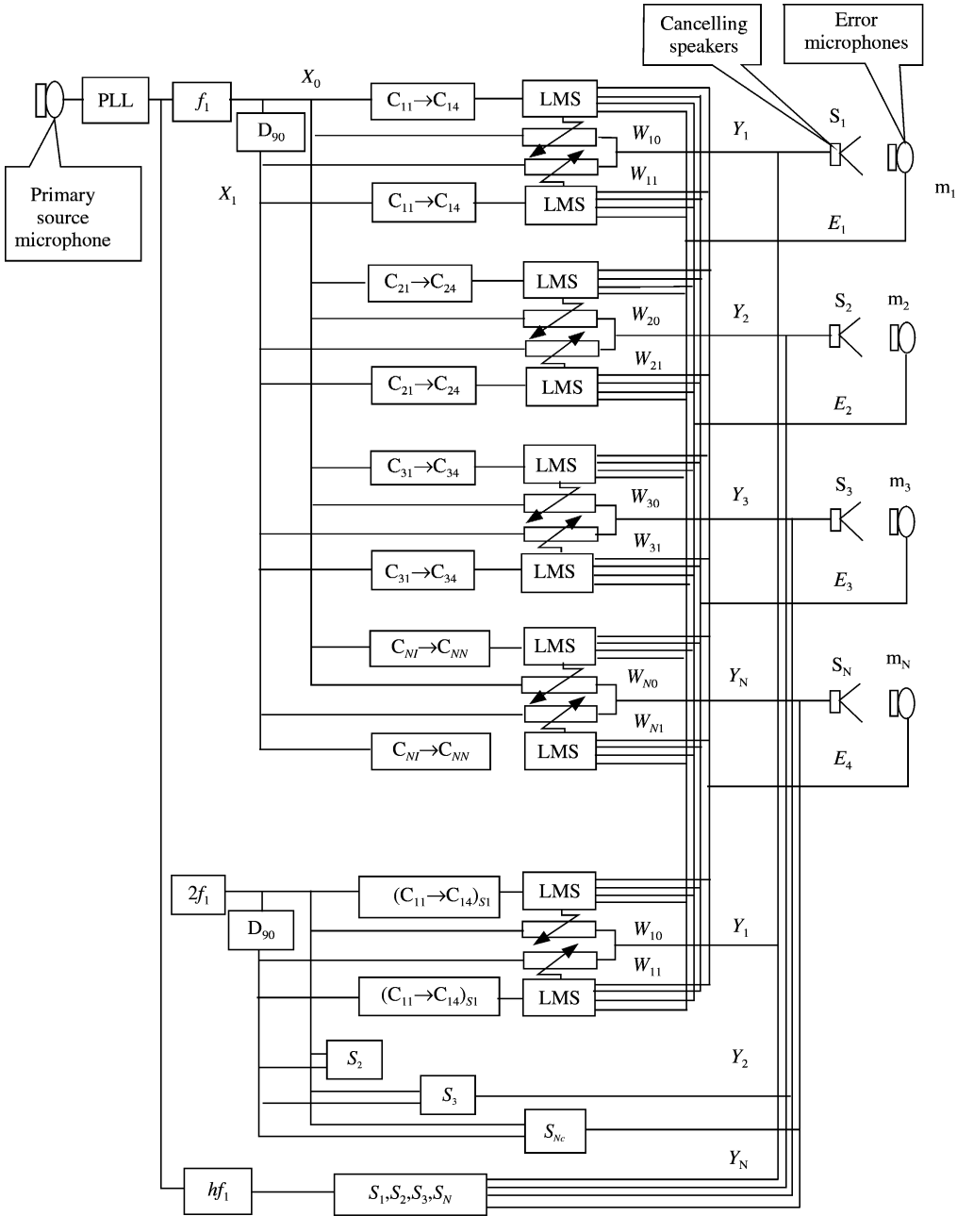

Figure 3. A multi-channel (N_c), multi-frequency (h) cancelling structure.

and for the N_cth channel

$$Y_{Nc} = W_{Nc0}X_0 + W_{Nc1}X_1,$$

$$W_{Nc0} = W_{Nc0} - \mu E_1 C_{Nc1}X_0 - \mu E_2 C_{Nc2}X_0 - \mu E_3 C_{Nc3}X_0, \ldots, -\mu E_{Nc}C_{NcNc}X_0,$$

$$W_{Nc1} = W_{Nc1} - \mu E_1 C_{Nc1}X_1 - \mu E_2 C_{Nc2}X_1 - \mu E_3 C_{Nc3}X_1, \ldots, -\mu E_{Nc}C_{NcNc}X_1, \quad (7)$$

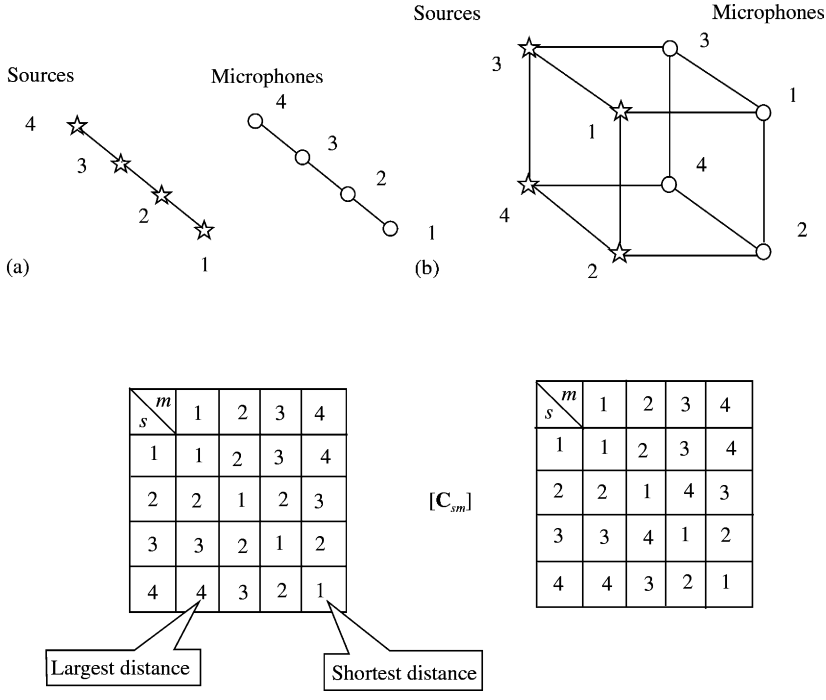

s \ m	1	2	3	4
1	1	2	3	4
2	2	1	2	3
3	3	2	1	2
4	4	3	2	1

s \ m	1	2	3	4
1	1	2	3	4
2	2	1	4	3
3	3	4	1	2
4	4	3	2	1

Figure 4. Matrix elements listed in successive propagation distances for (a) line source/microphone array and (b) square source/microphone array.

where μ is the adaptive step size. The propagation matrix elements C_{sm} depend on the geometry of the cancelling system as illustrated in Figure 4. For example, the propagation matrix is given for a line and rectangular system array, for four speakers and four microphones. In general there are N_c^2 propagation paths, but for a symmetrical system there are only N_c paths (four paths in this case with 1 representing the shortest and 4 the longest path). These paths are translated into initial propagation delays n_a (CPP in the program), measured in samples using white noise impulse response methods described in section 2.

For memory efficiency, these delays are represented in the computer program as successive pointers around a circular buffer; thus,

$$C_{sm}X_0 \rightarrow XBUF[CPP] \quad \text{in phase,} \quad C_{sm}X_1 \rightarrow XBUF[CP] \quad 90^\circ \text{ phase,}$$
$$CP = CPP + D_{90}, \quad \text{where } D_{90} = f_n/4f, \tag{8}$$

where f_n/f is the ratio of the sampling frequency to the cancelling frequency. The delays are written as a maximum sample value and difference values around the circular buffer.

3.2. OPERATING CONDITIONS

To operate these systems efficiently two conditions need to be met.

3.2.1. *Condition I. Stability robustness*

For a multi-channel multi-frequency freefield system to converge effectively, it is necessary to align all stability regions of that system for each cancelling frequency. There are

a series of stability bands, defined by orbital poles circulating around the system zeroes [4], for each control loop involving each source and detector propagation path combination. To maximize the adaptive performance of the complete system (maximum attenuation and minimum frequency distortion), it is necessary to operate each individual control loop in the centre of its stability band and align all stability bands of the system. The problem of centre band operation and stability-band alignment becomes more critical as the number of stability bands increase according to the square of the channel number.

The initial alignment of these stability bands and centre-band operation is achieved through adjusting the sample advance number (n_a) in the delayed LMS algorithm for each propagation path, according to equation (34) in reference [5] i.e.,

$$n_a = (N_s - N_{tf}) f_n/f, \quad N_{tf} = N_{em} - N_r, \quad N_r = r_{sm} f/c_0, \tag{9}$$

giving

$$n_a = ((N_s - N_{em}) f + r_{sm}/c_0) f_n. \tag{10}$$

Here f, f_n, r_{sm}, and c_0 are the acoustic frequency, sampling frequency, propagation distance between the speaker and microphone, and the speed of sound taken to be 340 m/s respectively. N_{tf} is the phase transfer function of the loop, N_{em} is the electromechanical phase transfer function, N_r is the propagation phase delay and N_s is the stability number of the loop in terms of the number of 2π radians.

For each propagation path, one can

(a) Measure N_{tf} automatically using, for example, white noise impulse testing techniques described in reference [5] (here it is necessary to perform frequency-domain analysis to obtain the phase response).
(b) Physically measure or calculate from geometry or use white noise impulse response to measure r_{sm}. Then, use previously measured or estimated N_{em}, which is representative of each stability loop.
(c) Calculate n_a for the smallest propagation distance (source–detector plane separation distance), then calculate Δn_a from Δr_{sm} using $\Delta n_a = \Delta r_{sm}(f_n/c_0)$, where Δr_{sm} is the difference in propagation paths.
(d) Initially calculate n_a from above. Then fine tune n_a and keep it tuned for environmental changes, automatically, to give maximum cancellation depth for each path. This can be implemented, for example, by minimizing the error E at the microphones, as previously mentioned, by minimizing the drive signal Y at the secondary sources or zeroing V at the input to the phase-lock loop, all of which indicate centre-band operation and therefore maximum cancellation depth.

3.2.2. *Condition II. Convertions robustness*

In large channel number freefield systems, it is found that a spectrum of instability peaks exist which have to be avoided if the system is to remain stable. The control robustness, for given frequencies, which basically deteriorates with increasing channel number, has to be maximized, based primarily on the physical hardware and system geometry.

For maximum convertions robustness, a multi-channel system should operate with a minimum eigenvalue spread. This can be expressed in terms of a matrix condition number K [17, 18] given by

$$K = \varepsilon_{max}/\varepsilon_{min}. \tag{11}$$

For maximum stability, K should be as small as possible. The eigenvalues ε are found from solving the matrix equation

$$\det [\varepsilon \mathbf{I} - \mathbf{C}^{\mathrm{H}}\mathbf{C}] = 0 \quad \text{or} \quad \varepsilon = \mathbf{C}^{\mathrm{H}}\mathbf{C}, \tag{12}$$

where $\mathbf{I}$ is the unit matrix, $\mathbf{C}$ is the propagation matrix and H denotes the transpose of the complex argument (Hermitian).

3.3. TWO-CHANNEL SYSTEM

It is found that a two-channel system is indicative of the properties of more complex systems. For freefield conditions, it is found that K has a series of instability peaks (maxima) as a function of the acoustic frequency, given by equation (75) of reference [5]. These peaks should be avoided if the adaptive system is to remain stable. The instability peaks occur when the path difference (Δr) between the secondary source and detection microphone distances are a multiple, p, of a half-acoustic wavelength, $\lambda/2$, of the primary source frequency f ($\lambda = c_0/f$, where c_0 is the speed of sound).

For example, a symmetrical two-channel system with propagation distances r between sources and microphones labelled 1 and 2 is

$$\Delta r = r_{12} - r_{11} = p\lambda/2 = pc_0/2f. \tag{13}$$

From simple geometry, if $c \gg ab$, where a and b represent the speaker–speaker and microphone–microphone separation distances and c is the separation distance between the two sets of transducers, then

$$r_{12} - r_{11} \approx ab/2c. \tag{14}$$

Thus from equations (13) and (14), a series of instability spectral peaks occur when

$$f_n \approx pc_0 c/ab, \quad p = 1,2,3, \ldots. \tag{15}$$

Also the corresponding K_p value for each peak, (all have the same K value for a two-channel system) can be determined from equation (72) of reference [5]

$$\varepsilon_{max} = (R_{12} + R_{11})^2, \quad \varepsilon_{min} = (R_{12} - R_{11})^2. \tag{16}$$

Here, the propagation amplitude term $R = \omega_n \rho_0/4\pi r = f_n \rho_0/2r$; ω_n is the angular source frequency, ρ_0 is the propagating fluid density and r is again the corresponding propagation distances between the speakers and microphones. From equation (11)

$$K_p = [(r_{12}/r_{11} + 1)/(r_{12}/r_{11} - 1)]^2. \tag{17}$$

Thus, the frequency f_1 at which the first instability peak occurs depends on the difference between the propagation distances ($r_{12} - r_{11}$), the larger the difference the lower the frequency. Whereas the stability strength ($1/K_p$ value at the peak) depends on the ratio of the propagation distances (r_{12}/r_{11}), the larger the ratio the smaller the eigenvalue spread the lower the K_p value and the stronger the system.

For example, the typical f_1 and K values for a parallel system (equal speaker–speaker spacing a and microphone–microphone spacing b where $a = b = 1$ m), as the distance between the speaker and microphone spacing c increases, are given in Table 1.

The table indicates that a squarish geometry ($c \approx a \approx b$) gives a low f_1 and correspondingly low K. A large c and a small a and b gives a high f_1 and an accompanying high K. The K values at which instability occurs depend on the cancelling strength as discussed later in section 4. Thus, the system geometry has to be optimized to avoid or

TABLE 1

Calculation of the first instability peak f_1 and the corresponding condition number K_p for a 2-channel system as c varies, $a = b = 1$ m

c(m)	0·5	1	2	4
$r_{12} - r_{11}$	0·62	0·4	0·24	0·12
r_{12}/r_{11}	2·24	1·4	1·1	1·03
f_1(Hz)	170	340	680	1360
K_p	10	40	400	4290

minimize the effect of the ill-conditioning peaks within the operating frequency range. Fortunately, the "DC" zero order conditioning peak f_0 (large value close to zero frequency) is stable. As both f_1 and K increase with increasing distance c or decreasing spacing a or b, then there is usually a practical choice. If f_1 is arranged to be above the cancellation frequency range of interest, its K value does not matter, or if f_1 is low within the operational frequency range, then K will be low and stability may be assured. However, intermediate distances could be a problem.

3.4. LARGE MULTI-CHANNEL SYSTEMS

The main computational steps in evaluating the exact situation for large multi-channel systems, using equation (11), are illustrated by

$$K(low\ f,\ upp\ f,\ incr\ f) := \left\| \begin{array}{l} ind \leftarrow 0 \\ \text{for } f \in low\ f,\ low\ f + incr\ f \cdots upp\ f \\ \quad \left\| \begin{array}{l} \omega \leftarrow 2 \cdot \pi \cdot f \\ k \leftarrow \omega / c_o \\ \text{for } n \in 0 \cdots 3 \\ C_n \leftarrow \mathrm{i}(\omega \cdot \rho / 4 \cdot \pi \cdot \hat{r}_{0,n}) \cdot \mathrm{e}^{\mathrm{i} \cdot k \cdot r_{0,n}} \\ \mathbf{M} \leftarrow \begin{bmatrix} C_0 & C_1 & C_2 & C_3 \\ C_1 & C_0 & C_3 & C_2 \\ C_2 & C_3 & C_0 & C_1 \\ C_3 & C_2 & C_1 & C_0 \end{bmatrix} \\ \Lambda \leftarrow \mathrm{eigenvals}(H(\mathbf{M}) \cdot \mathbf{M}) \\ K_{ind} \leftarrow \max(\Lambda)/\min(\Lambda) \\ ind \leftarrow ind + 1 \end{array} \right. \\ K \end{array} \right. \tag{18}$$

where ω is the angular acoustic frequency, k is the acoustic wave number, $\rho = 1{\cdot}21$ kg/m^3 is the density of air, $c_o = 340$ m/s is speed of sound, C_n are propagation element field strengths at an inverse propagation distance r between each secondary source and detection microphone, with a phase delay kr. Here n is the number of propagation paths $n = 0 \rightarrow 3$, there are four sources and four microphones giving 16 propagation distances, but only four different distances for a symmetrical system. $\mathbf{M}$ represents the propagation matrix of elements between the four different source and microphone combinations, Λ represents the eigenvalues, $\mathrm{H}(\mathbf{A}) := ((\vec{\mathbf{A}}))^{\mathrm{T}}$ is the Hermitian of the matrix i.e., the transpose T of the complex argument A, and K is the conditioning number, defined in equation (11).

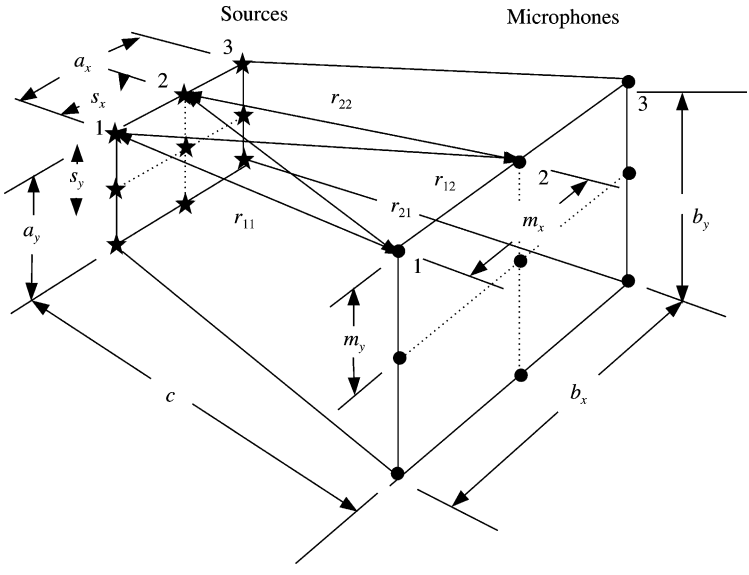

Figure 5. Source and microphone array geometry for a multi-channel system.

The simple equations (15) and (17) above can be used to assess the stability of more complex, larger channel number systems given by the exact equation (18). Of course, all the elements in the multi-channel matrix are coupled both mathematically and practically (acoustically), resulting in complex conditioning spectra. Fortunately, the eigenvalues in the two array directions can be treated approximately as uncoupled (independent), to obtain the major instability effects, as described below.

For a two-dimensional rectangular source and microphone array, in the x and y directions, the effective transducer spacing s_x, m_x and s_y, m_y replaces the overall array dimension, a_x, b_x and a_y, b_y as illustrated in Figure 5, then

$$(\Delta r)_x = (r_{21} - r_{11})_x = p_x(\lambda_n)_x/2 = \; p_x c_o/2(f_n)_x. \tag{19}$$

Again from geometry if $c \gg ab$

$$(r_{21} - r_{11})_x \approx s_x m_x/(2c),\; s_x = a_x(N_x - 1)^{-1/2}, \qquad m_x = b_x(N_x - 1)^{-1/2}, \tag{20}$$

where N_x is the channel number in the x direction. From equations (19) and (20) and assuming an equivalent set of equations in the y direction, one has

$$(f_n)_x \approx p_x c_o c\; (N_x - 1)/(a_x b_x), \quad (f_n)_y \approx p_y c_o c(N_y - 1)/(a_y b_y). \tag{21}$$

It is found that the eigenvalues are only weakly coupled between the source directions. Thus the spectral instability peaks $(f_p)_x$, for a linear array of "cancellers" and detectors in the x direction can be found to be a first order independently of the $(f_p)_y$ instability peaks in the y direction, and vice versa. Of course in reality, the situation is much more complex with interference between the spectral peaks corresponding to the complete set of eigenvalues.

Figure 6 gives the detailed computed instability peaks for various sizes of rectangular source and microphone array planes separated by $c = 2{\cdot}81$ m, using the exact solution, equations (18). Figure 6(a) is for a 4-channel (2×2-array; two channels in each of the x and y directions) system where $a_x = b_x = 1$ m. It shows a series of instability peaks corresponding to multiples of $(f_1)_x \approx 1$ kHz, where equation (21) gives $(f_1)_x = 955$ kHz. In

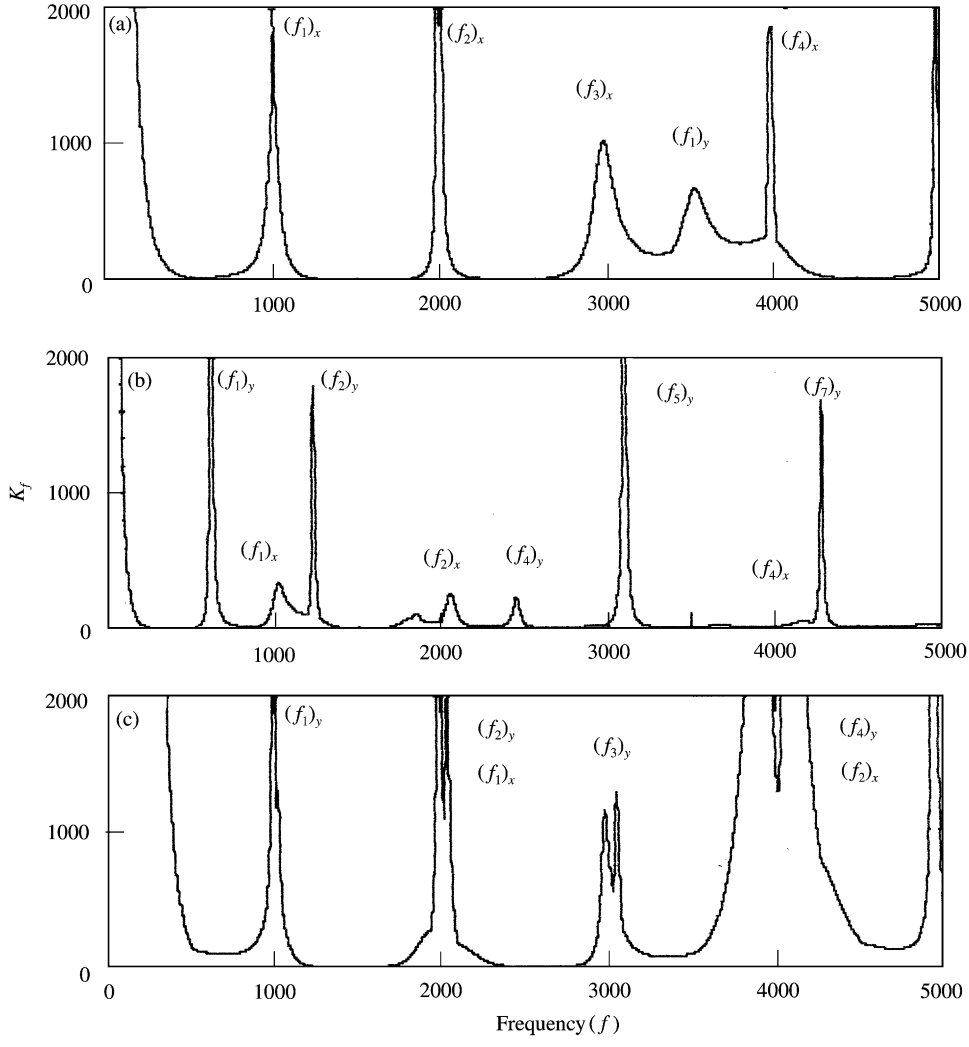

Figure 6. Instability spectra (condition number K_p versus frequency f) for (a) a 2×2-channel no. system where $a_x = b_c = 1$ m, $a_y = b_y = 0{\cdot}23$ m, $c = 2{\cdot}81$ m; (b) 2×2-channel where $a_x = b_x = 1$ m, $a_y = b_y = 1{\cdot}3$ m, $c = 2{\cdot}81$ m; (c) 3×2-channel where $a_x = b_x = 1$ m, $a_y = b_y = 1$ m, $c = 2{\cdot}81$ m.

the y direction, $a_y = b_y = 0{\cdot}5$ m computing $(f_1)_y \approx 3{\cdot}5$ kHz, here equation (21) gives $(f_1)_y = 3{\cdot}4$ kHz. There is some complex interference between $(f_1)_y$ and $(f_3)_x$ (thickening of the base and reducing the $(f_3)_x$ peak value), but basically the instability peak positions are estimated independently in each of the x and y directions.

Figure 6(b) shows again a 2×2-array but this time $a_y = b_y = 1{\cdot}3$ m. The corresponding $(f_1)_y$ peak separation now shrinks to multiples of about 600 Hz, compared to the 3·5 kHz previously, and from equation (21) $(f_1)_y = 563$ kHz. The $(f_1)_x \approx 1$ kHz peaks remain approximately in the same position as in Figure 6(a), although very much diminished in size. Thus, the lower stability peaks tend to dominate the spectrum as in the previous figure. Figure 6(c) shows a 3×2-channel array (three channels in the x direction and two in the y direction). The $(f_1)_y \approx 1000$ Hz peaks correspond to $a_y = b_y = 1$ m for the two channels in the y direction. The $(f_1)_x \approx 2$ kHz peaks corresponds to the three channel spacing in the x direction over the same $a_x = b_x = 1$ m, i.e., the frequency has now doubled according to

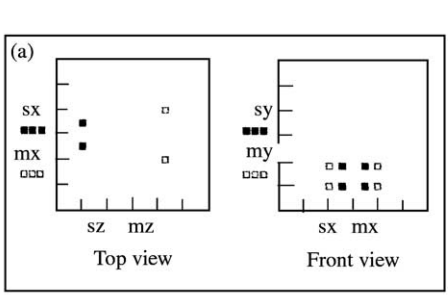

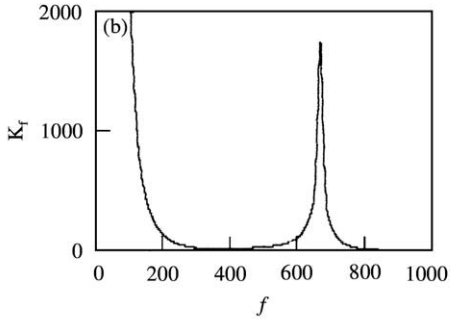

(c)

N	f (Hz)	n_a	Stability bands in Hz (0 400 800)
−1	200	68 69 71 72	
−1	400	58 59 61 62	
−1	600	54 55 57 58	
−1	800	51 52 54 55	
−1	1000	49 50 52 53	
−2	200	48 49 51 52	
−2	400	48 49 51 52	
−2	600	47 48 50 51	
−2	800	46 47 49 50	
−2	1000	45 46 48 49	
−3	200	28 29 31 32	
−3	400	38 39 41 42	
−3	600	40 41 43 44	
−3	800	41 42 44 45	
−3	1000	41 42 44 45	
−4	200	8 9 11 12	
−4	400	28 29 31 32	
−4	600	34 35 37 38	
−4	800	36 37 39 40	
−4	1000	37 38 40 41	

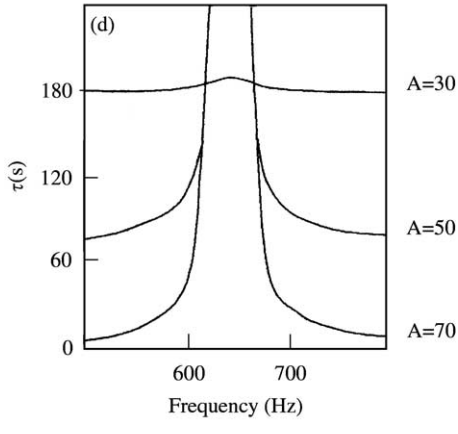

Figure 7. Laboratory system geometry, resulting conditioning spectra and measured stability bands: (a) laboratory system geometry; (b) resulting conditioning spectra; (c) calculated sample advance numbers (n_a) and measured stability bands as a function of frequency f and stability band no, N; (d) measured instability peak with adaptive time constant, τ versus frequency for three reference amplitudes A(mV), $\mu = 0{\cdot}001$.

$N_x - 1 = 2$, i.e., the peak now corresponds to the transducer spacing, not the transducer array size.

3.5. MEASURED ROBUSTNESS

Figure 7(a) illustrates the geometry of a 4-channel (2×2) system installed in the laboratory, where s and m indicate the secondary (cancelling) sources and microphones respectively. The graduations in the figure are in meters. In the horizontal x direction, the speaker separation is $a_x = 0{\cdot}9$ m, the microphone separation is $b_x = 2$ m and the two lines of transducers are separated in the z direction by $c_z = 3{\cdot}28$ m. In the vertical y direction, the speakers and microphones are separated by $a_x = b_x = 0{\cdot}8$ m. The corresponding propagation path lengths between the sources, s, and microphones, m, are given by

$$sx = \begin{bmatrix} -Ds/2 \\ -Ds/2 \\ Ds/2 \\ Ds/2 \end{bmatrix}, \quad mx = \begin{bmatrix} -Dm/2 \\ -Dm/2 \\ Dm/2 \\ Dm/2 \end{bmatrix}, \quad sy = \begin{bmatrix} Hs2 \\ Hs1 \\ Hs2 \\ Hs1 \end{bmatrix}, \quad my = \begin{bmatrix} Hm2 \\ Hm1 \\ Hm2 \\ Hm1 \end{bmatrix}, \quad mz = c, \quad sz = 0, \tag{22}$$

$$r_{s,m} = \sqrt{(mx - sx)^2 + (mz - sz)^2 + (my - sy)^2}, \quad s = 0 \cdots 3 \quad m = 0 \cdots 3. \tag{23}$$

where Ds, Hs and Dm, Hm are the horizontal and vertical dimensions of the source and microphone, respectively, centred about the origin. This gives 16 paths with four different distances $r_{00} = 3{\cdot}33$ m, $r_{01} = 3{\cdot}42$ m, $r_{02} = 3{\cdot}59$ m and $r_{03} = 3{\cdot}67$ m.

Figure 7(b) gives the resulting conditioning spectra (condition number versus frequency) for the geometry given in Figure 7(a). It can be seen that the resulting spectrum has a first peak of about 1800 situated at about 600 Hz, dominated by the larger x direction dimensions. Equation (21) for the $(f_1)_x$ and $(f_1)_y$ gives 619 and 1742 Hz respectively.

Figure 7(c) shows the calculated n_a numbers using equation (10), for each of the four different propagation distances r_{sm} between the speakers and microphones given by equation (23). These are calculated for a particular acoustic frequency f, stability region number N and electromechanical transfer function N_{em}, measured using white noise impulse techniques. The corresponding measured stability regions are plotted as a function of acoustic frequency. It can be seen that there is a vertical blank column centred at about 600 Hz, where no stability bands exists. It can be seen that an instability peak of magnitude 1800 situated at about 600Hz, shown in Figure 7(b), allows no adaptive convergence. Figure 7(c) shows the measured instability peaks as a function of adaptive time τ in seconds and reference amplitude A in millivolts. Low A gives long adaptive convergence time τ, sufficiently large A results in the peaks becoming unstable (infinite τ), with a complex structure within the peak (not shown here). Obviously, these peaks need to be avoided for an effective control system.

4. ADAPTIVE PERFORMANCE

After establishing the conditions for freefield cancellation systems to perform efficiently, the adaptive convergence speed of these systems is now considered.

4.1. SINGLE CHANNEL

The adaptive speed of a single-channel system was considered in reference [4]. The adaptive time constant τ_a (time for the error to decay 63% of its initial value) and the adaptive step size μ in the LMS algorithm were measured at the centre of their stability band for various levels of reference input amplitude A. The resulting rectangular hyperbolic relationship was established as

$$\tau_a \beta = \kappa, \quad \beta = \mu A^2, \tag{24}$$

where κ is an adaptive performance constant whose value depends on the system hardware, the smaller the κ value the smaller the adaptive time. β is the cancelling source strength, the larger its value the smaller the adaptive time and the faster is its response. Also, the stability bandwidth shrinks as β increases, until finally becoming zero at β_{zbw}, as discussed in detail in reference [4]. The primary source power amplifier PA could be varied arbitrarily between 0 and 8. Its power was adjusted to keep fairly constant sound pressure at the microphone for various distances and frequencies. The secondary source power amplifier SA could be varied also between 0 and 8. However, as SA lies within the adaptive loop it affects β_{zbw}, τ_a and the κ values as shown in Table 2.

Most of the measurements in reference [4] were made using SA = 4. These were carried out for various levels of A, from 10 mV to 1 V, secondary source–microphone propagation distances $r_{sm} = 1$, 2 and 4 m and acoustic cancelling frequency $f = 200$, 400 and 800 Hz. The

TABLE 2

Reference signal for zero bandwidth A_{zbw} and the corresponding cancelling source strength β_{zbw} as a function of secondary source-power amplifier SA for $f = 400$ Hz, $\mu = 0{\cdot}1$, and $PA = 2$. Also, shown is the adaptive time constant τ_a and adaptive performance constant κ for $A = 80\,mV$, $\mu = 0{\cdot}02$, $\beta = 0{\cdot}13 \times 10^{-3}$ and $r_{sm} = 1$ m

SA	1	2	3	4
A_{zbw}(mV)	630	330	128	100
$\beta_{zbw}(\times 10^{-3})$	40	10	1·6	1
τ_a(samples)	2300	1000	200	100
$\kappa(\times 10^{-3})$	300	130	16	10

primary source was a 0·1 m diameter speaker housed in a small enclosure with its own built in amplifier. Equation (24) then becomes

$$\tau_a \beta (r_{sm})^g (f/400)^h = \kappa, \tag{25}$$

where r_{sm} and f were normalized on 1 m and 400 Hz respectively. The powers g and h were found to be approximately -1 and $-1/2$, respectively, where negative powers indicate increasing adaptive times. It is found that $\kappa \approx 10 \times 10^{-3}$ for τ_a measured in samples and $\beta_{zbw} \approx 0{\cdot}8 \times 10^{-3}$. In addition, there are propagation distance delays τ_p, given by $n_r = (r_{sm}/c_0) f_n$, before any adaptive process can start. For the above three distances, these are 12, 24, and 48 samples, or 3, 6, and 12 ms (τ_p/f_n, $f_n = 4000$ Hz). Thus, the total convergence time is given by

$$\tau_t = \tau_a + \tau_p. \tag{26}$$

Generally, τ_p is much smaller than τ_a, except for very large β, also large r_{sm} makes both τ_a and τ_p large, so τ_a will usually dominate the response time.

4.2. MULTI-CHANNELS

For the study of multi-channel systems, a primary source baffle board $L_p = 1$ m, 0·5 m, and 0·25 m long $\times$ 0·3 m high was used containing 4 m, 2 m, and one nominally 0·25 m diameter speakers respectively. The secondary sources were again 0·1 m diameter speakers housed in small enclosures with their own power amplifies, the same sources as used in the single-channel study. Table 3 shows the adaptive performance constant $\kappa(\times 10^{-3})$ for a parallel propagation distance $r_{sm} = 2$ m (0° shadow angle) and an acoustic frequency $f = 400$ Hz, for the three baffle board primary source sizes $L_p = 1$, 0·5, and 0·25 m and for $s = 1$, 2, 4 and 6 secondary sources. For better cancellation depth, the secondary source power amplifier was reduced from SA $= 4 \rightarrow 2$.

For one baffled 0·25 m primary source and one housed 0·10 m secondary source, it was found that $\kappa = 460 \times 10^{-3}$ for $r_{sm} = 2$ m ($\kappa \approx 230 \times 10^{-3}$ for $r_{sm} = 1$ m), whereas for the single-channel measurements, using both housed 0·1 m primary and secondary source speakers, $\kappa = 130 \times 10^{-3}$ at $r_{sm} = 1$ m and SA $= 2$, i.e., the smaller speaker had the lower κ and therefore has the faster response (smaller time constant), as anticipated. It can be seen from Table 3 that κ dramatically decreases with increasing secondary source number, decreasing the adaptive time (approximate to the inverse square of s for $L_p = 0{\cdot}5$ m). Also, increasing the size of the primary source has only a moderately increasing effect on κ.

TABLE 3

Adaptive performance constant $\kappa(\times 10^{-3})$ *versus primary source size* L_p *and number of secondary sources s.* $r_{sm} = 2$ m, $f = 400$ Hz, $SA = 2$

L_p(m)	1	2	4	6
0·25	460	58	—	—
0·5	480	122	26	—
1	480	230	38	16

TABLE 4

Adaptive performance constant $\kappa(\times 10^{-3})$ *versus acoustic frequency f for three propagation distances* r_{sm} *and three primary source sizes* $L_p = 0{\cdot}25$, 0·5 *and* 1 m. $s = 4$, $SA = 2$

	f(Hz)								
	200			400			800		
L_p(m)	0·25	0·5	1·0	0·25	0·5	1·0	0·25	0·5	1·0
r_{sm}(m)									
1	12	—	13	13	—	22	16	—	38
2	23	19	19	26	26	38	38	58	77
4	45	—	32	51	—	64	77	—	128

Table 4 shows the adaptive performance constant κ versus acoustic frequency f and propagation distance r_{sm} for three primary source sizes $L_p = 0{\cdot}25, 0{\cdot}5$ and 1 m. It can be seen that κ doubles approximately with doubling in r_{sm} and f, for large L_p considerable increasing the adaptive time. Also that κ increases more strongly with increases in L_p at the higher acoustic frequency f.

The data in Tables 3 and 4 indicate the following relationship for the adaptive performance constant κ, extending equation (25) generally to

$$\tau_a \beta (r_{sm})^g (f/400)^h (N_c)^i (L_p)^j (\alpha + 1)^k = \kappa, \tag{27}$$

where N_c, L_p and α are the number of cancelling sources, primary source size and the shadow control angle in the x direction respectively. The dominant powers can be represented approximately by $g \approx -1, h \approx -1, i \approx 2, j \approx -1/2$ whereas $k \approx -0{\cdot}1$ is small, particularly at low frequency. β_{zbw} for $Nc = 2$, 4, 6 is approximate 3·4, 0·36, 0·053 $(\times 10^{-3})$ respectively. β_{zbw} increases with increases in frequency and propagation distance r_{sm}. Of course, the relationships between the parameters are more complex than expressed above. However, equation (27) does give an indication of the relative importance between them.

Figure 8 shows the simultaneous adaptive decay for a $3 \times 2 = 6$-channel system. The data were taken with a 1 m baffled primary source containing four 0·25 m speakers. The microphone separation distance $L_m = 1$ m at a secondary speaker–microphone distance of $r_{sm} = 2$ m and a primary source–secondary source separation distance $r_{ps} = 0{\cdot}3$ m. The reference amplitude was 80 mV, the adaptive step size $\mu = 0{\cdot}025$, secondary source amplifier SA = 2 and primary source amplifier PA = 2. The figure shows the cancelling speaker drive signals (Y) on the left hand side and the microphone error signals (E) on the right hand side of the figure, for all six channels. The access of 12 channels of simultaneous data from the

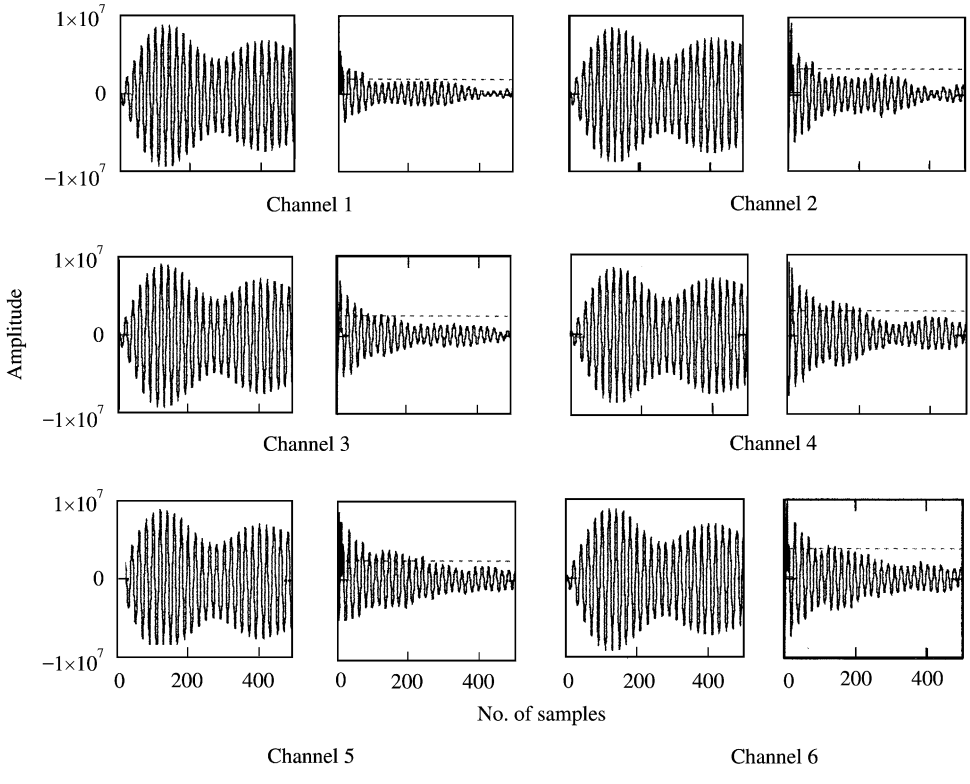

Figure 8. Adaptive convergence close to instability, showing individual simultaneous speaker drive and microphone error signals for each channel. Number of channels $N_c = 6(3 \times 2)$, $f_{mod} = 14$ Hz, $f_n = 4000$ Hz, $f = 200$ Hz, $A = 80$ mV, $\mu = 0{\cdot}025$, $\beta = 160 \times 10^{-6}$, $r_{ps} = 0{\cdot}3$ m, $r_{pm} = 2$ m, $L_p = 1$ m, $L_m = 1$ m, SA = 2, PA = 2.

DSP to the host processor was a challenge, which required considerable software development skills. In the centre of a wide stability band, the error signals decay in near-perfect exponentials, which is not very interesting graphically. However, for a cancellation strength of $\beta = \mu A^2 = 0{\cdot}016 \times 10^{-3}$, close to the zero stability bandwidth β_{zbw}, the signals show oscillations indicating the onset of instability. A modulation frequency of $f_{mod} = 200/14 \approx f_{n/n} = 4000/300 = 14$ Hz is clearly seen, resulting in sideband frequencies each side of the cancelling frequency, as considered in detail in reference [4].

5. ACOUSTIC PERFORMANCE

To compare the acoustic performance of real hardware implemented adaptive systems with theory, the sound pressure characteristics were computed using acoustic wave equations used to establish the acoustic properties in references [1, 2]. The system dimensions were chosen so that the acoustic characteristics could be computed and then compared with the measurements made in the laboratory. These measurements were then, in turn, used to validate the theory and then to predict the shadows at large distances.

5.1. COMPUTED SOUND FIELDS

The following acoustic fields were computed using an array of point acoustic monopole sources and the acoustic wave equation. Both the primary source to be cancelled and the

secondary sources used to cancel the primary acoustic fields were modelled using these point acoustic sources.

The number of primary sources used was two and four, arranged horizontally, with overall spacing of 0·35 and 0·75 m respectively. There was a duplicate row of sources arranged vertically above the first row, separated by 0·1 m to produce a shallow vertically shadow angle γ.

The microphones were arranged in a vertical rectangular plane, in two rows 0·5 m apart vertically, either $L_m = 1$ or 2 m apart horizontally and placed at $r_{pm} = 2$ m distance from the primary source. This forms a vertical shadow elevation angle, equivalent to $\gamma \approx 5^\circ$. The corresponding set of azimuthal shadow angles in the horizontal plane are $\alpha \approx 8^\circ$, 20° for $L_p = 0{\cdot}35$ and 0·75 m for $L_m = 1$ m and $\alpha \approx 40^\circ$, 50° for the same L_p and $L_m = 2$ m respectively. The secondary sources were then placed within the shadow control angles at $r_{ps} = 0{\cdot}1$ m from the primary source.

To calculate the shadow depth, it is first necessary to compute the sound pressure from the primary source alone. Figure 9 shows the computed sound pressure contours plotted in decibels, in 5 dB steps. The distance axes are graduated in meters. The computations are for a primary source alone for two effective primary source sizes $L_p = 0{\cdot}35$ m containing two sources (figures (a–c)) and $L_p = 0{\cdot}75$ m with four equally spaced sources (figures (d–f)). These are computed for three source frequencies 200, 400 and 800 Hz. At low frequencies (200 Hz), the radiation is almost omnidirectional (equal in all directions), particularly for the smaller source.

As the frequency increases, the sound pressure reduces towards $\varphi = \pm 90^\circ$ (plane of the source), until the first interference minima of the major lobe appears at less than 90°. These minima, generated by acoustic interference between the discrete sources, are given by $\varphi = \sin^{-1}[\lambda/L_p(N_p/(N_p - 1))]$ as predicted by equations (A45) and (A46) in reference [2]. Here, λ is the acoustic wavelength and N_p is the number of discrete primary sources within the source length L_p. These first minima are 37, 25 and 58° for Figure (a), (d) and (e) respectively. The minima of course occur first for the larger source dimension as the frequency increases.

Figure 10 shows the cancelled primary source field for a 2×2 secondary-source cancelling array. Again, the primary source sizes are $L_p = 0{\cdot}35$ and 0·75 m and the three acoustic source frequencies are $f_{ac} = 200$, 400 and 800 Hz. The primary–secondary source distance $r_{ps} = 0{\cdot}1$ m and the microphone separation distance is $L_m = 1$ m, giving shadow control angles of $\alpha \approx 20$ and 8°, for the two source sizes, respectively. At low frequencies, the cancelled regions are wider than the control angles. In fact, the cancelled regions can be 360° giving a net all round reduction (net secondary source absorption). This can be seen to be true, for example, if Figures 10(f) and 9(f) are compared. Whether net absorption occurs depends on the primary–secondary source separation distance r_{ps} compared to the acoustic wavelength λ. For $r_{ps} = 0{\cdot}1$ m and acoustic frequency $f = 200$, 400 and 800 Hz, the corresponding $\lambda/r_{ps} = 17$, 8·5 and 4·25 respectively. Thus for $\lambda/r_{ps} > 8{\cdot}5$ ($f < 400$ Hz), there is net absorption. For $\lambda/r_{ps} \gg 4$, the directivity tends to be tripole-like (cardoid), when $\lambda/r_{ps} \approx 4$ and 2 the directivity tends to become dipole-like (figure-of-eight) and quadrupole-like (four-leaf clover, not applicable here) respectively.

As the frequency increases the cancelled region becomes progressively confined within the control angles. Also, the shadow depth decreases as the wavelength λ approaches the secondary source separation distance $d_s \approx L_p/(N_s - 1)$, where N_s is the number of secondary sources and $L_p \approx L_s$. Thus cancellation systems that have similar λ/d_s should, all things being equal, have similar cancellation depths. For example, Figures 10(a) and (e) and 10(b) and (f) each have similar λ/d_s which are $\approx 1{\cdot}2$ and $\approx 2{\cdot}3$, respectively. Comparing with the corresponding uncancelled field in Figure 9, their respective shadows are approximately $130–115 = 15$ dB and $130–100 = 30$ dB at an observation distance

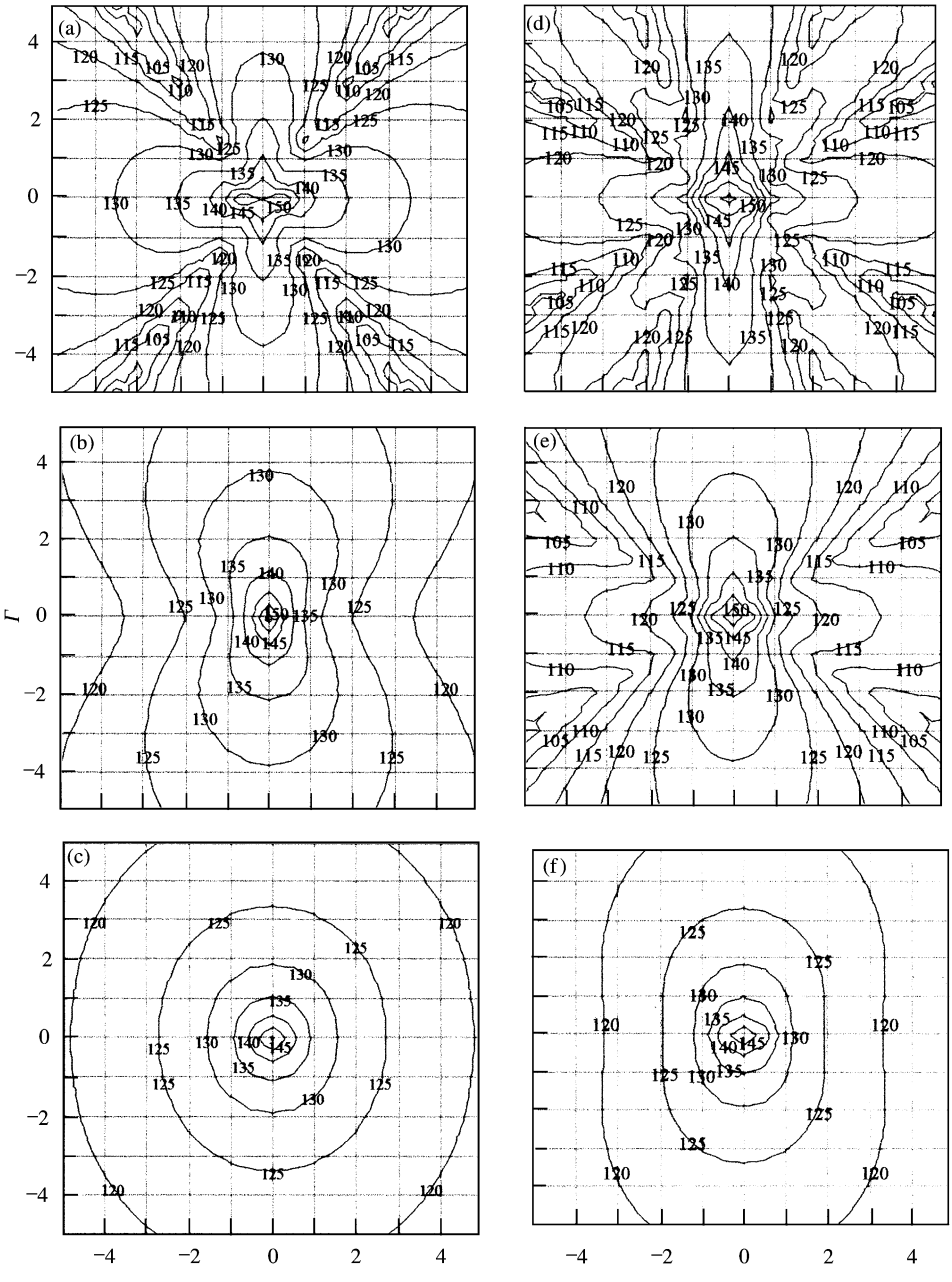

Figure 9. Uncancelled primary source $L_p = 0{\cdot}35$ m ($P = 2$) for (a) 800 Hz, (b) 400 Hz, and (c) 200 Hz and with $L_p = 0{\cdot}75$ m ($P = 4$) for (d) 800 Hz, (e) 400 Hz and (f) 200 Hz.

$r_{p0} = 4$ m. In Figure 10(d), λ/d_s is less than unity (0·56) giving negligible shadow depth as predicted by equation (A48) in reference [15]. Here, for example, the dipole-like directivity ($\lambda/r_{ps} = 4{\cdot}12$) is clearer, it gives minimum sound to both the front and rear and a maximum to the sides.

Figure 11 shows the computed shadows for a 3×2 secondary-cancelling source array for a microphone separation distance $L_m = 2$ m, making the control angles $\alpha \approx 50$ and 40° for the smaller and larger source sizes respectively. Again, this figure shows similar trends to

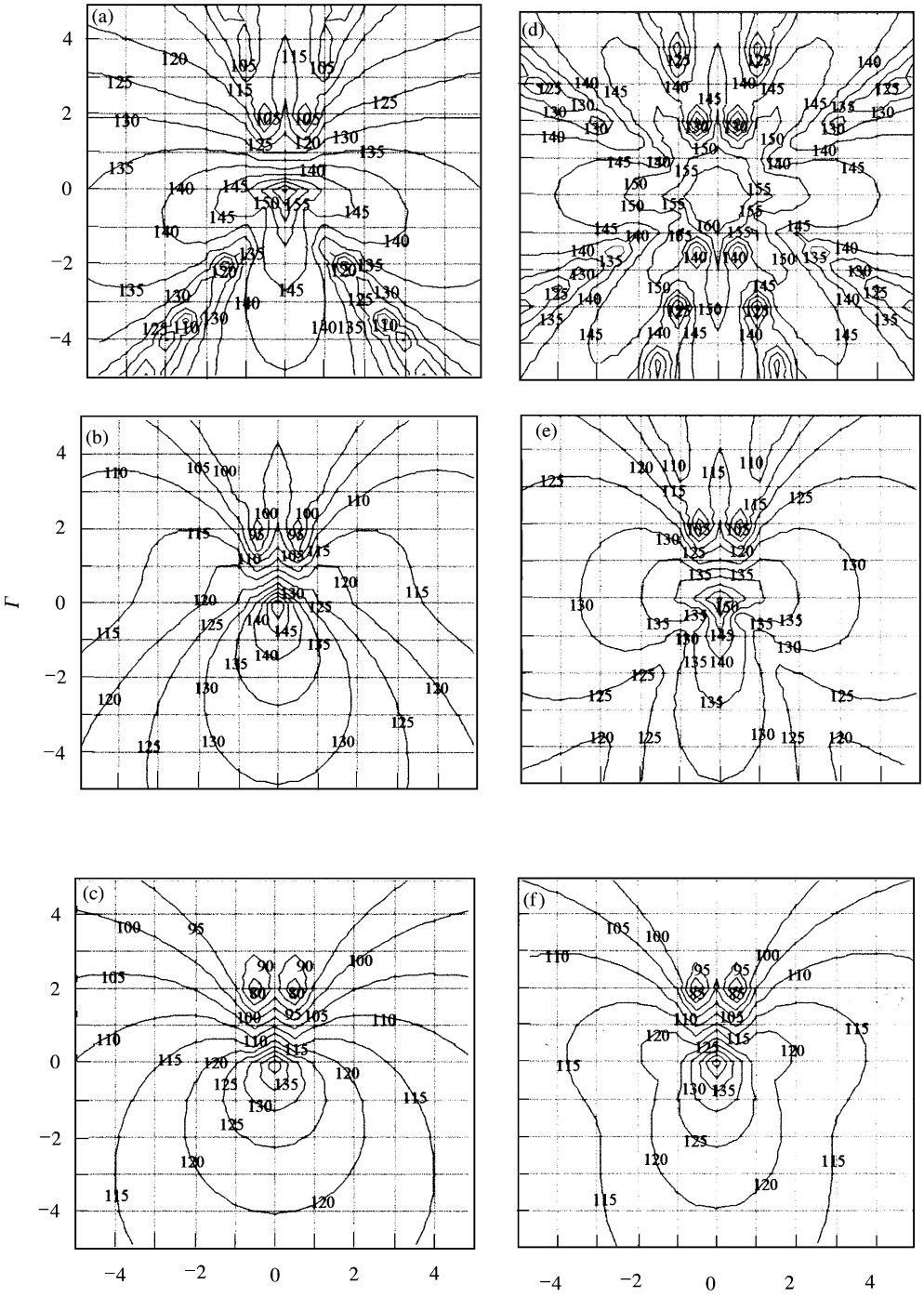

Figure 10. Cancelled primary source $N_c = 2 \times 2$, $L_p = 0{\cdot}35$ m, $P = 2$ for (a) 800 Hz, (b) 400 Hz, (c) 200 Hz and with $L_p = 0{\cdot}75$ m, $r_{ps} = 0{\cdot}1$ m, $P = 4$ for (d) 800 Hz, (e) 400 Hz and (f) 200 Hz. The microphone plane $L_m = 1$ m $\times H_m = 0{\cdot}5$ m is situated at $r_{pm} = 2$ m giving shadow angles of $\alpha = 20$ and 8° for the two source sizes respectively.

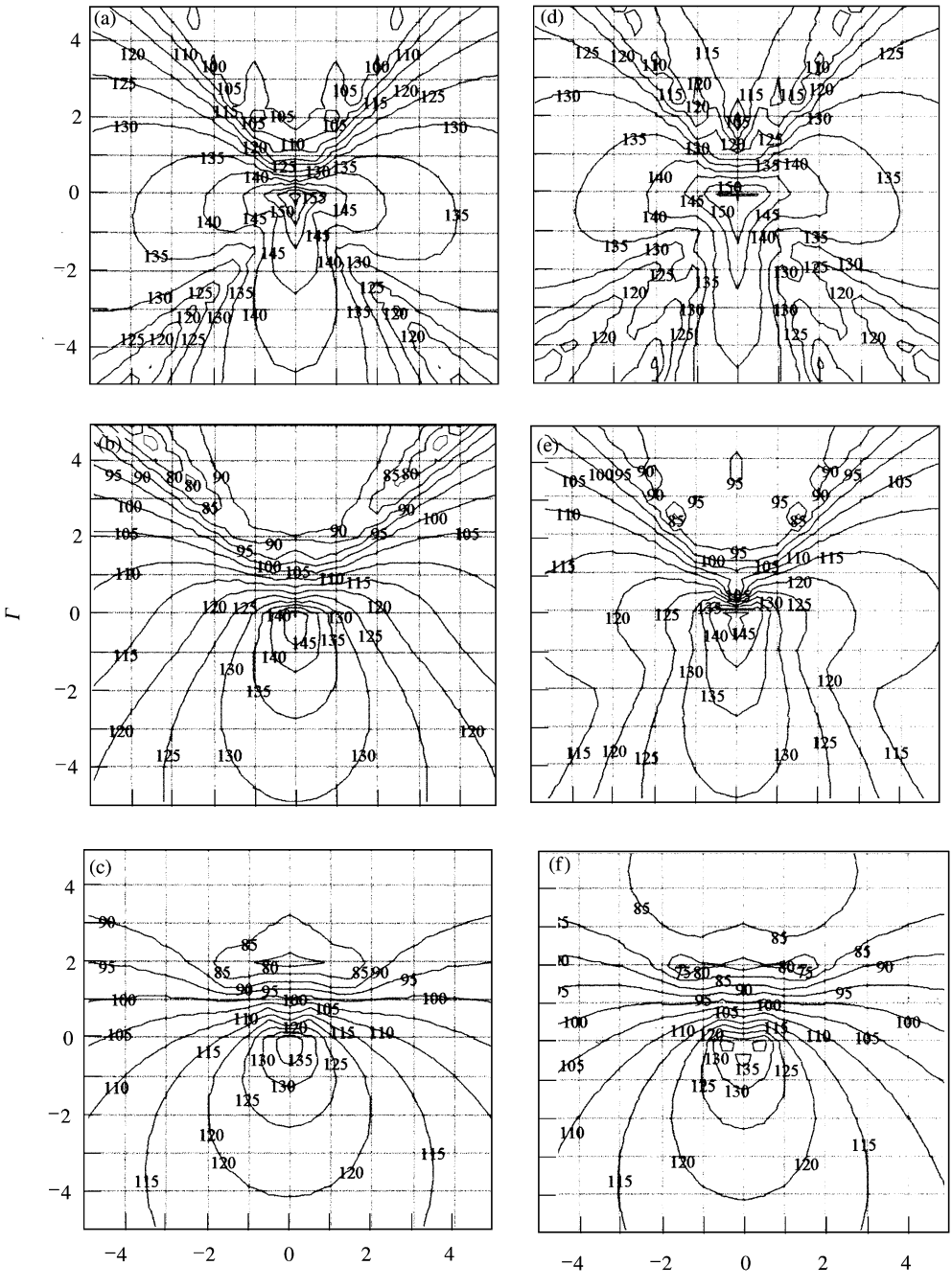

Figure 11. Cancelled primary source $N_c = 3 \times 2$, $L_p = 0{\cdot}35$ m, $P = 2$ for (a) 800 Hz, (b) 400 Hz, (c) 200 Hz and with $L_p = 0{\cdot}75$ m, $r_{ps} = 0{\cdot}1$ m, $P = 4$ for (d) 800 Hz, (e) 400 Hz, $c = 200$ Hz. The microphone plane $L_m = 2$ m $\times H_m = 0{\cdot}5$ m is situated at $r_{pm} = 2$ m giving shadow angles of $\alpha = 50$ and 40° also $\beta = 9^\circ$.

Figure 10, with the shadow angles being well formed at the higher frequency and all round attenuation at the lower frequency. However, because the secondary source spacing d_s is now smaller (halved), the shadow depths are potentially greater. For Figures 11(a) and (e)

and 11(b) and (f), the λ/d_s ratios are now approximately 2·4 and 4·6, giving cancellation over larger shadow angles, i.e., approximately 30 and 40 dB, respectively, at $r_{p0} = 4$ m. Figure 11(d) now has a $\lambda/d_s = 1{\cdot}1$ giving a shadow of approximately 20 dB.

5.2. MEASURED ACOUSTIC SHADOWS

In sections 3 and 4, the necessary control conditions have been established to obtain optimum cancellation performance from implemented hardware systems. The resulting acoustic fields from these systems are now considered. The sound pressure directivity measurements were made in a laboratory, whose floor area is 6 m × 6 m and height 5 m. The walls, floor and ceiling were covered with 10 cm thick panels of fibre glass, density 4·3 kgm/m^3, giving a nominal 95% absorption above 200 Hz.

To obtain acoustic measurements over at least $r_{p0} = 4$ m, the primary source was placed in the corner of the laboratory. The cancellation performance was documented in the horizontal x direction. A similar cancellation effect was assumed in the vertical y direction. Fixed observation microphones were placed over a horizontal arc of $\varphi = 90^\circ$ at zero vertical angle $\gamma = 0$ at $r_{p0} = 4$ m distance from the primary source. The data were taken with a sampling frequency of 4 kHz and plotted automatically with in-house developed software.

The primary sources used initially in the study were generated using a baffle board $L_p = 0{\cdot}5$ and 1 m in length times 0·3 m high, consisting of 2 and 4, 25 cm loudspeakers respectively. These dimensions were equivalent acoustically to 0·35 and 0·75 m, as calculated from the primary source directivity alone. Unfortunately, the open baffle board produced a dipole-type directivity (the sound pressure from the front and back of the speakers interfered producing a minimum sound pressure in the baffle board plane $\varphi = 90^\circ$). Therefore, the board was replaced by individual "monopole sources". These were 0·1 m speakers housed in separate enclosures placed at the same equivalent distances, i.e., $L_p = 0{\cdot}35$ and 0·75 m. These individual sources were more omnidirectional, but not as powerful as the larger baffled sources resulting in poorer cancellation performance at lower frequencies. Otherwise, measurements were made corresponding to the geometry in the computations.

Figure 12 shows the measured sound pressure directivity in decibels for the 0·35 m long primary source (a–c) and the 0·75 m primary source (d–f). A 2 × 2-channel cancelling system was used with microphones $L_m = 1$ m apart horizontally and primary–microphone distance $r_{pm} = 2$ m, giving control angles $\alpha \approx 20$ and 8° for the two source sizes respectively. As already mentioned, observer measurements were made over $\varphi = 0 \rightarrow 90^\circ$ at a distance of $r_{p0} = 4$ m and mirrored over the other 90°.

The dotted lines in the figure show the primary source directivity alone for the three acoustic frequencies $f = 200$, 400 and 800 Hz. The directivities were generally as predicted by the computations in Figure 9, bearing in mind that the presence of the cancelling structure (secondary speakers and support stands) affects the primary source directivity alone. The sound was largest in front of the source $\varphi = 0^\circ$, reducing to the side, $\varphi = 90^\circ$. The first minima, are only approximately as predicted by the computations. The full line shows the measured sound pressure cancellation level for the same three frequencies. Generally, the shadow depths reduce as the frequency and the primary source size increase. At 200 and 400 Hz, in front of the source, the shadow depths are about 20 and 15 dB compared with the computed values of 30 and 15 dB respectively. At 800 Hz, $L_p = 0{\cdot}75$ m, Figure 12(d), the cancellation is very small (≈ 5 dB) in agreement with the computation.

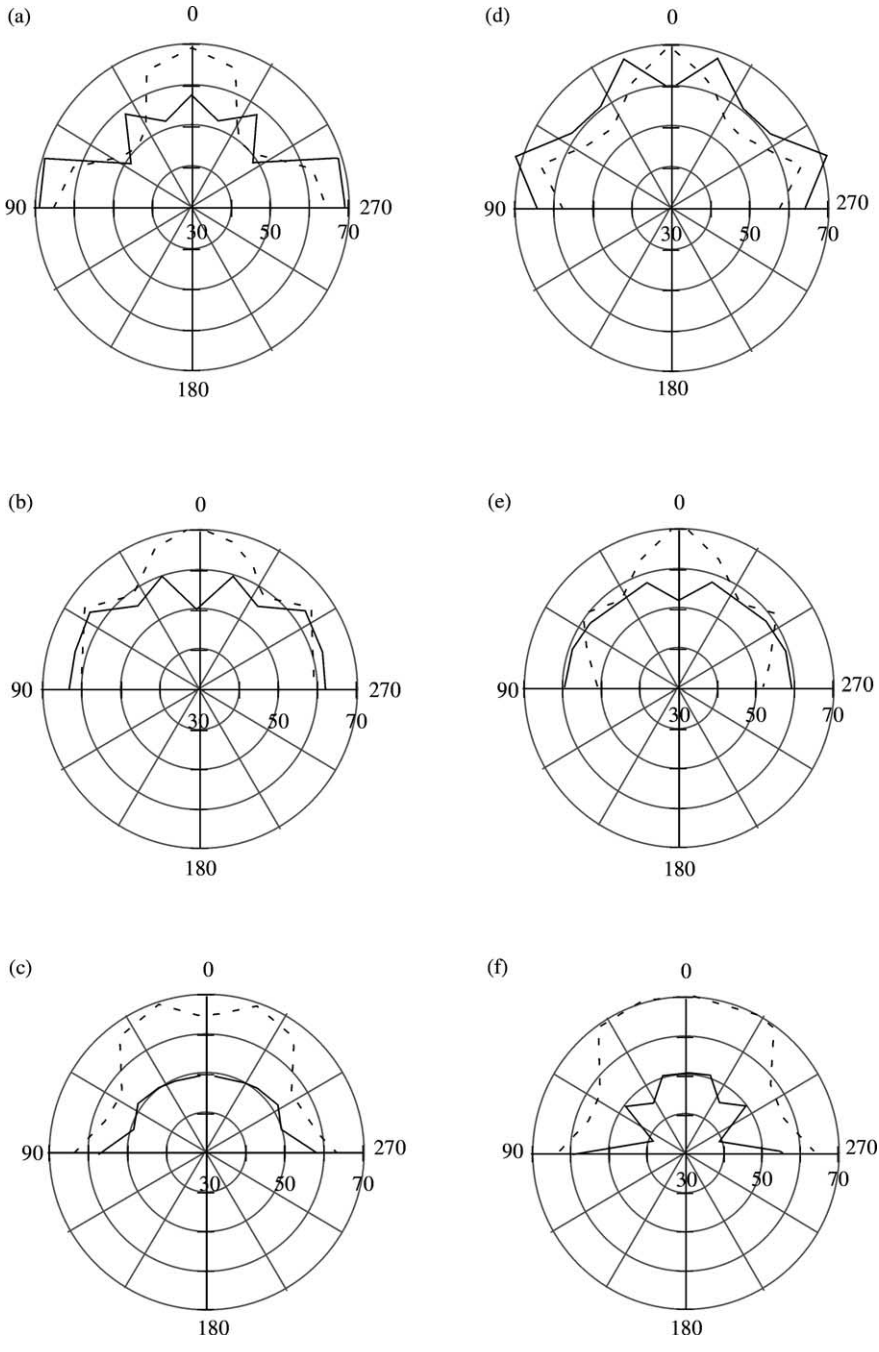

Figure 12. Measured directivity of the 2×2 system having primary source sizes $L_p = 0{\cdot}35$ m for (a) 800 Hz, (b) 400 Hz, (c) 200 Hz and with $L_p = 0{\cdot}75$ m $L_p = 2{\cdot}0$ m for (d) 800 Hz, (e) 400 Hz, (f) 200 Hz. $L_m = 1$ m, $r_{sm} = 2$ m, $r_{ps} = 0{\cdot}15$ m, $A = 80$ mV, $\mu = 0{\cdot}001$, SA $= 1{\cdot}75$ and PA $=$ varied. – – –, uncancelled field; ——, cancelled field.

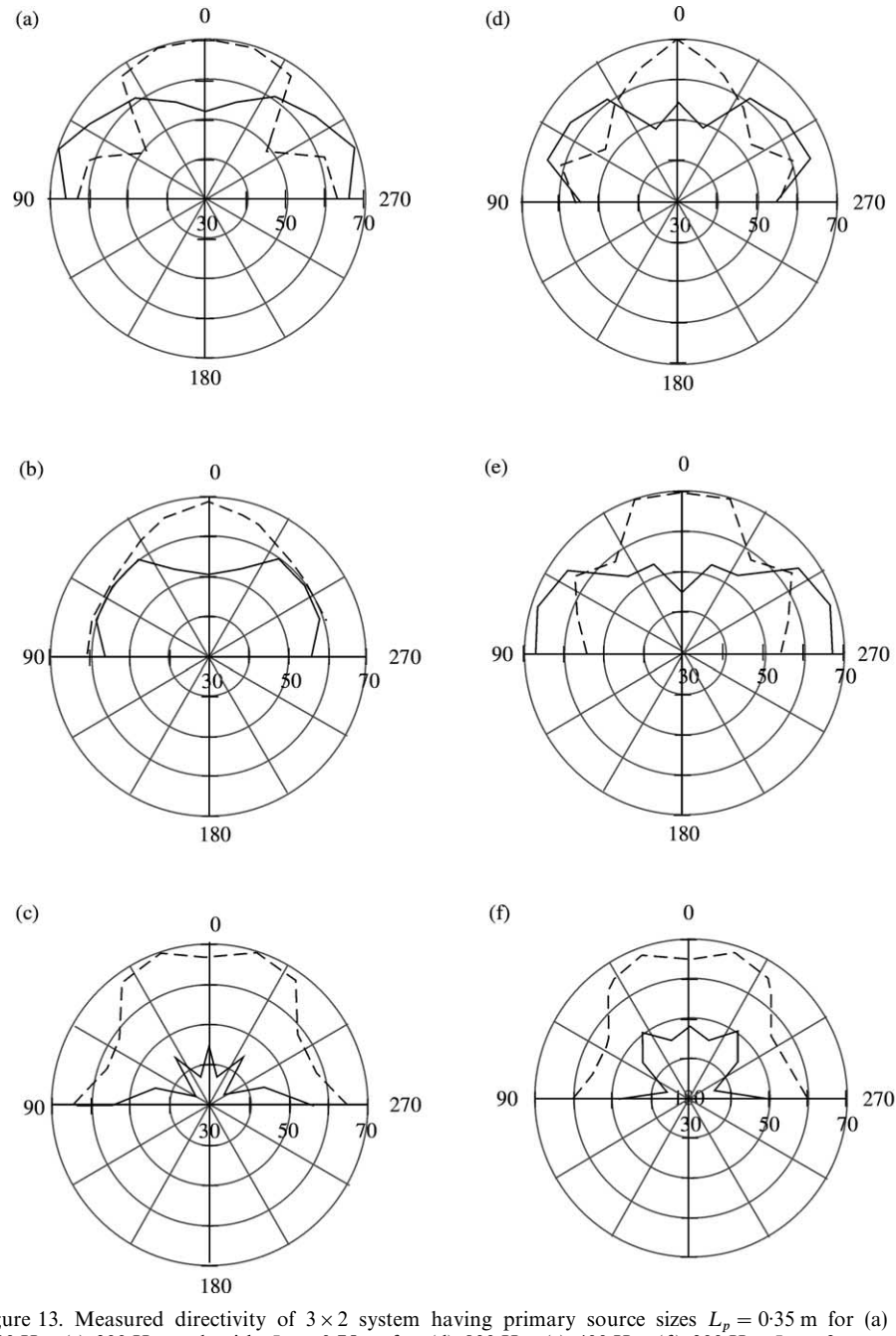

Figure 13. Measured directivity of 3×2 system having primary source sizes $L_p = 0{\cdot}35$ m for (a) 800 Hz, (b) 400 Hz, (c) 200 Hz and with $L_p = 0{\cdot}75$ m for (d) 800 Hz, (e) 400 Hz, (f) 200 Hz. $L_m = 2$ m, $r_{sm} = 2$ m, $r_{ps} = 0{\cdot}15$ m, $A = 80$ mV, $\mu = 0{\cdot}001$, SA = 1·75 and PA = varied. – – –, uncancelled field; ——, cancelled field.

This is because the secondary source separation $d_s \approx L_p = 0{\cdot}75$ is larger than the acoustic wavelength $\lambda = 0{\cdot}42$ ($\lambda/d_s = 0{\cdot}56$)

Figure 13 shows the sound pressure directivity for a 3×2-channel cancelling system for an increased microphone spacing of $L_m = 1$–2 m, giving azimuthal shadow control angles of

$\alpha \approx 50$ and 40° for the smaller and larger source sizes respectively. The full line again gives the cancelled field. The figure shows similar trends to Figure 12 and the computation Figure 11, with the shadow angles being well formed at the higher frequency and all round attenuation at the lower frequency. However, because the secondary source spacing d_s is now smaller (halved), the shadow depths are potentially greater. For the frequencies 200, 400, and 800 Hz, they are approximately 25, 20 and 15 dB compared with the predictions of 40, 30 and 20 dB. As mentioned previously, the baffled primary source gave a better cancellation performance at low frequency by about 10 dB. The cancelling structure also affected the primary source directivities alone.

5.3. FARFIELD PREDICTIONS

The forgoing measurements and predictions have been confined to the laboratory dimensions (5 m × 5 m). The good agreement between measurement and prediction gives confidence in both the measurements and the computer prediction program. This program is now used to indicate acoustic properties at large distances from the source.

Figure 14 shows computed shadows at, $r_{p0} = \pm 500$ m, from a primary source $Lp = 0{\cdot}75$ m, for a 3×2-cancelling system and three frequencies 200, 400 and 800 Hz. The shadow angles horizontally are $\alpha = 40^\circ$ and vertically $\gamma = 9^\circ$. The sound pressures are calculated for the uncancelled source and the cancelled source for primary–secondary source distances $r_{ps} = 0{\cdot}1$ and $0{\cdot}4$ m and primary source–microphone distances $r_{pm} = 2$ and 20 m.

The sound pressure levels are approximately 40 dB lower than those in Figures 9 and 11 according to the 100-fold increase in the propagation distance. Row (a) in Figure 14 for the uncancelled field is exactly 40 dB lower than those in the corresponding Figures 9(d–f). The swirls are a figment of computation resolution that can be removed with increased resolution at the expense of an increase in computation time.

Comparing row (b) with row (a) in Figure 14, the first significant point is that the interference zeros in the uncancelled field have been completely removed, i.e., the shadows have formed successfully across these complex sound fields containing 180° phase reversals. The second point to note is that the shadow depths at $r_{p0} = 400$ m are $85–55 \approx 40$, $90–60 \approx 30$ and $95–75 \approx 20$ dB for $f = 200$, 400 and 800 Hz respectively. These levels are similar to the corresponding difference values of $125–85 \approx 40$, $130–95 \approx 35$ and $135–115 \approx 20$ dB at $r_{p0} = 4$ m in Figure 9(d–f), and Figure 11(d–f), indicating that the shadow depth is basically unaltered with distance. The third point is that row (c) demonstrates that the shadow depth increases (approximately 20 dB for all three frequencies) with increasing primary source–microphone distances of 10 times, $r_{pm} = 2$ to 20 m.

The fourth point is that row (d) shows that the shadow decreases with increasing primary–secondary source distance r_{ps} but still gives deeper shadows (6 dB for all three frequencies) than those in row (b). Here $\lambda/r_{ps} = 4{\cdot}25$, $2{\cdot}12$ and $1{\cdot}06$ for $f = 200$, 400 and 800 Hz, respectively; giving sound reduction to the sides, for 400 and 800 Hz, corresponding to the quadrupole-like directivity. In conclusion, it can be said that individual dimensions are not important, it is the ratio with the acoustic wavelength λ that counts. The primary source size L_p, the primary–secondary source distance r_{ps}, the primary source–microphone distance r_{pm} and the secondary source spacing $d_s = L_p/(N_c - 1)$, where N_c is the number of channels, are all important compared to λ.

Finally, it should be stressed that these computed properties indicate only the major propagation characteristics. In reference [3], it is shown as to how the cancellation system is affected with the detailed effects of complex three-dimensional primary sources, ground

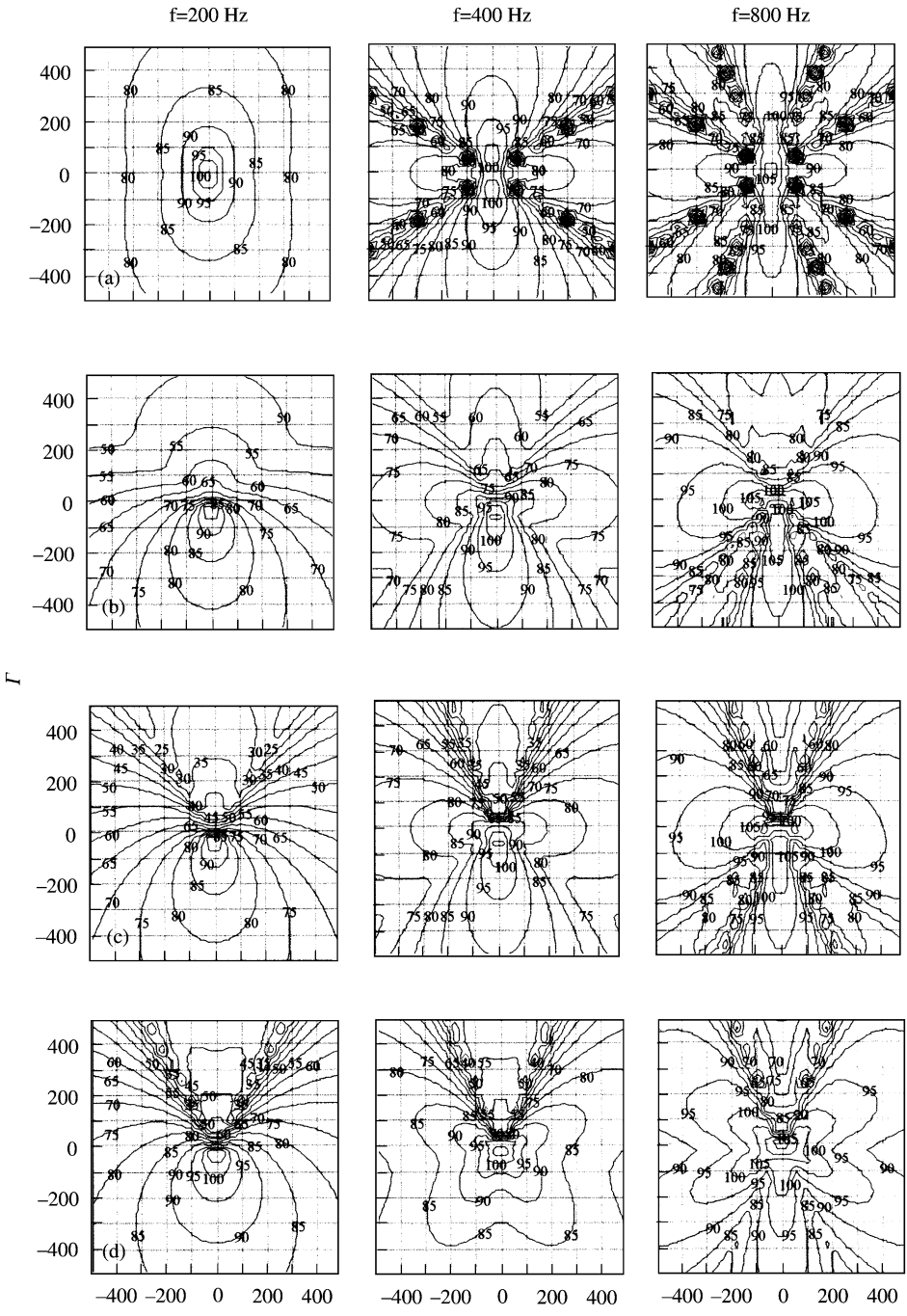

Figure 14. Acoustic shadow calculated at large distances from the source $r_{p0} = \pm 500$ m, $N_c = 3 \times 2$, $L_p = 0{\cdot}75$ m ($P = 4$), $\alpha = 40^\circ$, $\beta = 9^\circ$ for three frequencies $f = 200$ Hz, 400 Hz and 800 Hz: (a) uncancelled source; (b) $r_{ps} = 0{\cdot}1$ m, $r_{pm} = 2{\cdot}0$ m; (c) $r_{ps} = 0{\cdot}1$ m, $r_{pm} = 20{\cdot}0$ m; (d) $r_{ps} = 0{\cdot}4$ *m*, $r_{pm} = 20{\cdot}0$ m.

reflection and steady cross winds. In reference [6], the effect of transient environmental changes such as reflections from moving surfaces and varying wind on the stability of the adaptive process is considered. More complex propagating medium effects such as

turbulence, varying temperature gradients, absorption and non-linear effects on the cancellation performance are not considered.

6. CONCLUSIONS

The acoustic properties of the fundamental "canceller" (phase-controlled dipole) established in reference [4] are used in this paper to understand and establish the detailed characteristics of multi-channel systems. Bundles of these fundamental cancelling units, contained within shadow control angles, have been demonstrated to produce deep acoustic shadows across complex acoustic fields from large non-compact sources.

Optimum performance is obtained from these systems through two conditions. Condition I is that for a multi-channel, multi-frequency, freefield system to converge effectively, it is necessary to align all stability regions of that system. There are a series of stability bands for each control loop involving each source and detector propagation path combination. To maximize the adaptive performance of the complete system (maximum attenuation, minimum adaptive time and minimum frequency distortion), it is necessary to operate each individual control loop in the centre of its stability band and align all stability bands of the system. Equations developed for automatic alignment of these stability bands have shown to give accurate prediction in the implementations of these control systems.

Condition II is that to maintain convergence of large channel number systems, large eigenvalue spread (large maximum to minimum eigenvalue ratios, K, of the total control system) must be avoided. It is found that K has a series of instability peaks corresponding to path differences between the secondary sources and detection microphones of multiples of acoustic half wavelengths of the source frequency. The frequency at which the first instability peak occurs depends on the difference between these propagation distances, the larger the difference the lower the frequency. Whereas the convergence strength, $1/K$ value at the peak, depends on the ratio of the propagation distances, the larger the ratio the smaller the eigenvalue spread the lower the K value and the stronger the system.

The stability bandwidth of these freefield adaptive systems shrinks according to the signal strength $\beta = \mu A^2$, where μ is the adaptive step size and A is the reference signal amplitude. Towards the edge of the stability bands, satellite pole frequencies beat with the cancelling frequency zeros producing amplitude modulation and unwanted sideband frequencies. At the centre of the stability bands, the spectrum is pure and the adaptive time is shortest. Here, it is found that the adaptive time is inversely proportional to the square of the channel number, resulting in a huge increase in adaptive speed as the channel number increases. The adaptive time is also approximately proportional to the propagation distance between the secondary sources and the detection microphones, the acoustic frequency and the square root of the primary source size.

The theoretical shadow performance of these systems was also investigated. It is found that shadows were formed all around the primary source (reductions around 360°), providing the acoustic wavelength compared to the primary–secondary source distance ratio $(\lambda/r_{ps}) > 8$. For smaller values, the shadow becomes well defined within the shadow control angles. The directivities outside the shadows becoming predominantly tripole (cardiod), dipole (figure-of-eight) and quadrupole (four-leaf clover) resemblance for $(\lambda/r_{ps}) \gg 4$, ≈ 4, ≈ 2 respectively. The shadow depths increase with increasing channel number for (λ/d_s), greater than $\approx 0{\cdot}5$ where d_s is the cancelling source separation distance.

Measurements made in the laboratory are in good agreement with the theoretical predictions validating the theory. This theory, within the limitations assumed, can be used to predict the shadow characteristics over large distances in open air situations. Here, it is

found that the shadow properties are maintained at considerable distances including the very important shadow depth, paving the way for the development of commercial systems.

POST SCRIPT

This work is sponsored by the Department of Trade and Industry (SMART award) and protected by patent application PCT/GB01/00775

REFERENCES

1. S. E. WRIGHT and B. VUKSANOVIC 1996 *Journal of Sound and Vibration* **190**, 565–585. Active control of environmental noise.
2. S. E. WRIGHT and B. VUKSANOVIC 1997 *Journal of Sound and Vibration* **202**, 313–359. Active control of environmental noise, II: non-compact acoustic sources.
3. S. E. WRIGHT and B. VUKSANOVIC 1999 *Journal of Sound and Vibration* **222**, 635–668. Active control of environmental noise, IV: practical extensions to ECAS theory.
4. S. E. WRIGHT and H. ATMOKO 2001. *Journal of Sound and Vibration* **245**, 581–609. Active control of environmental noise, VI: performance of a fundamental free-field cancelling system.
5. S. E. WRIGHT and B. VUKSANOVIC 1999 *Journal of Sound and Vibration* **220**, 469–496. Active control of environmental noise, III: implementation of theory into practice.
6. S. E. WRIGHT and H. ATMOKO 2001 *Journal of Sound and Vibration* **244**, 107–122. Active control of environmental noise, V: the effect of environmental change on the stability of free-field sound cancelling systems.
7. P. LUEG 1936 *U.S. Patent, No.* 2043, 416. Process of silencing sound oscillations.
8. H. F. OLSON and E. G. MAY 1953 *Journal of the Acoustical Society of America* **25**, 1130–1136. Electronic sound absorber
9. G. B. B. CHAPLIN and R. A. SMITH 1979 *U.K. Patent* 1, 555–760. Improvements in and relating to active methods for attenuating compression waves.
10. B. WIDROW and S. D. STEARNS 1985 *Adaptive Signal Processing*. Englewood Cliffs, NJ, U.S.A. Prentice-Hall.
11. S. J. ELLIOTT, I. A. STOTHERS and P. A. NELSON 1987 *IEEE Transactions on Acoustic, Speech and Signal Processing* **ASSP-35**, 1423–1434. A multiple error LMS algorithm and its application to the active control of sound and vibration.
12. S. E. WRIGHT and O. L. ANGEVINE 1990 *Inter-Noise* 90, *The* 1990 *International Conference on Noise Control Engineering, Gothenburg, Sweden*. Active cancellation of hum of a simulated electric transformer.
13. S. M. KUO and D. R. MORGAN 1996 *Active Noise Control Systems*. New York, U.S.A.: John Wiley.
14. S. J. ELLIOTT 2001 *Signal Processing for Active Noise Control*. London: Academic Press.
15. J. ENCINAS 1993 *Phase Locked Loops*. London: Chapman & Hall.
16. R. E. BEST 1997 *Phase Locked Loops*. McGraw-Hill: New York.
17. S. LAFLIN 1988 *Numerical Method in Linear Algebra*. London: Chartwell-Bratt.
18. B. STEPHAN 1997 *Matrix Methods for Engineers and Scientists*. London: McGraw-Hill.